

Resolving Node Identifiability in Graph Neural Processes via Laplacian Spectral Encodings

Zimo Yan¹, Zheng Xie¹, Chang Liu¹, Yuan Wang²

¹National University of Defense Technology, Changsha, China.

²School of Urban Design, Wuhan University, Wuhan, China.

{yanzimo20, xiezheng81, nudt_liuchang_1997}@nudt.edu.cn, 2024282090042@whu.edu.cn

Abstract—Message passing graph neural networks are widely used for learning on graphs, yet their expressive power is limited by the one-dimensional Weisfeiler–Lehman test and can fail to distinguish structurally different nodes. We provide rigorous theory for a Laplacian positional encoding that is invariant to eigenvector sign flips and to basis rotations within eigenspaces. We prove that this encoding yields node identifiability from a constant number of observations and establishes a sample-complexity separation from architectures constrained by the Weisfeiler–Lehman test. The analysis combines a monotone link between shortest-path and diffusion distance, spectral trilateration with a constant set of anchors, and quantitative spectral injectivity with logarithmic embedding size. As an instantiation, pairing this encoding with a neural-process style decoder yields significant gains on a drug–drug interaction task on chemical graphs. When tested empirically on a challenging Drug-Drug Interaction (DDI) prediction task, improving both the area under the ROC curve and the F1 score and demonstrating the practical benefits of resolving theoretical expressiveness limitations with principled positional information.

Keywords:Laplacian Positional Encoding, Node Identifiability, Laplacian spectral

I. INTRODUCTION

Learning effective representations from graph-structured data is a fundamental challenge with profound implications across numerous domains, from molecular chemistry and drug discovery [1] to social network analysis and recommendation systems [2]. Graph Neural Networks (GNNs) have emerged as the dominant paradigm for this task, employing an iterative message-passing scheme to capture local neighborhood structures [3]. More recently, the integration of GNNs into probabilistic frameworks like Graph Neural Processes (GNPs) [4], [5] has unlocked new capabilities. By learning a distribution over functions on graphs, GNPs can not only make predictions but also quantify their own uncertainty, a feature that is invaluable for safety-critical applications and few-shot learning scenarios where data is scarce.

The predominant approach for constructing GNPs involves using a standard GNN, such as a Graph Convolutional Network (GCN) or GraphSAGE, as the primary encoder [6].

This work was supported by the National Natural Science Foundation of China [61773020] and the Graduate Innovation Project of National University of Defense Technology [XJQY2024065]. The authors would like to express their sincere gratitude to all the referees for their careful reading and insightful suggestions.

*Corresponding author: Zheng Xie (xiezheng81@nudt.edu.cn).

These models, which we categorize as Weisfeiler-Lehman GNPs (WL-GNPs), first generate a deterministic embedding for each node and then aggregate them to produce a global representation of the graph. This representation is subsequently used by the neural process to condition its predictions. While this combination is powerful, the resulting model inherits all the intrinsic limitations of its underlying GNN encoder.

A well-documented deficiency of standard GNNs is that their expressive power is fundamentally bounded by the 1-Weisfeiler-Lehman (1-WL) test for graph isomorphism [7], [8]. This theoretical ceiling means that WL-GNPs are incapable of distinguishing between certain non-isomorphic graph structures, a failure that is particularly pronounced in regular or highly symmetric graphs. Within the GNP framework, this limitation translates into a critical problem of *node indistinguishability*. If the encoder cannot differentiate two nodes based on structure, it will produce identical representations, leading to ambiguous posteriors and a provably high Bayes risk for tasks that depend on identifying a specific node’s role or position.

Motivation: This fundamental limitation of standard models raises a critical research question: *Can we design a Graph Neural Process that provably overcomes the expressive limitations of the 1-WL test, thereby resolving the issue of node indistinguishability and reducing the inherent Bayes risk?*

To address this challenge, we turn to the concept of positional encodings (PEs), which have been successfully used to inject positional awareness into permutation-invariant architectures like the Transformer [9]. Inspired by recent work leveraging the graph Laplacian spectrum to create robust node positions [10], we propose a new class of models, the Laplacian Graph Neural Process (Lap-GNP). Instead of relying on flawed local structures, Lap-GNP equips each node with a sign-invariant positional encoding derived from the Laplacian eigenvectors, providing a global “coordinate system”. In this work, we provide a rigorous theoretical proof that this principled approach allows Lap-GNP to achieve constant-shot identifiability on random regular graphs, a setting where we prove WL-GNPs are guaranteed to fail. We then empirically validate our theory on a challenging Drug-Drug Interaction (DDI) prediction task, demonstrating that the theoretical boost in expressiveness translates directly into significant gains in performance and sample efficiency.

Outline & Primary Contributions: This paper is organized

as follows. Section II provides a review of related work on graph neural networks and positional encodings. Section III introduces the necessary preliminaries, notations, and problem formulation. Section IV presents our core theoretical analysis, establishing the lower bound for WL-GNPs and the upper bound for Lap-GNPs. Section V describes the experimental setup and presents empirical results and provides an in-depth discussion of model behavior, connecting our theoretical findings to practical performance. Section VI concludes the paper and outlines potential directions for future work.

The primary contributions of this work are as follows:

- 1) We formally characterize the failure of standard GNN-based encoders (WL-GNPs) within a probabilistic setting, proving they suffer from a high Bayes risk due to node indistinguishability on symmetric graphs.
- 2) We propose the Laplacian Graph Neural Process (Lap-GNP), a novel model class that incorporates a sign-invariant spectral positional encoding to resolve structural ambiguity. We prove a formal sample-complexity separation, showing Lap-GNP achieves constant-shot identifiability where WL-GNPs fail.
- 3) We provide compelling empirical validation on a real-world Drug-Drug Interaction (DDI) prediction task, demonstrating that our theoretically-grounded Lap-GNP significantly outperforms standard baselines, thus bridging the gap between expressiveness theory and practical application.

II. LITERATURE REVIEW

A. Graph Representation Learning on Graph-Structured Data

Learning on graphs underpins node-, edge-, and graph-level tasks, including structural role discovery, link prediction, and molecular property prediction [1], [11], [12]. Message-Passing Graph Neural Networks (MPNNs) have become the prevailing paradigm: nodes iteratively aggregate neighborhood information to form task-specific representations [1], [7]. Representative instances span GCN [3], GraphSAGE [11], GAT [13], and GIN [7], with numerous architectural refinements [9], [14]. Despite empirical success, three challenges recur. First, expressiveness is bounded by the 1-Weisfeiler–Lehman (1-WL) test [7], [8], which renders many non-isomorphic but structurally similar subgraphs indistinguishable. Second, deeper stacks suffer *over-smoothing*, where embeddings homogenize across large regions [15], [16]. Third, long-range dependencies are compressed through narrow channels, leading to *over-squashing* [17], [18]. Remedies include higher-order or subgraph variants [8], [19], diffusion-augmented propagation [20], [21], and graph transformers that relax strict locality via attention [10], [22], [23]. These often trade accuracy for efficiency on sparse graphs unless complemented with principled positional priors.

B. Neural Processes and Graph Neural Processes

Neural Processes (NPs) model distributions over functions conditioned on context observations, combining amortized inference with GP-like uncertainty [4], [6]. Variants expand

representation capacity via attention and hierarchical latents [6], [24]. On graphs, Graph Neural Processes (GNPs) instantiate NP encoders with GNN backbones to capture relational structure, enabling few-shot generalization and calibrated predictive uncertainty in relational domains. In practice, most GNPs inherit the expressiveness ceiling of their underlying MPNN encoders and thus exhibit posterior ambiguity on symmetric graphs due to 1-WL limits [7], [8]. Complementary probabilistic graph models, such as VAEs on graphs [25], [26] and Bayesian GNNs [27], underscore the value of uncertainty for reliable decision-making, yet few works connect positional design to probabilistic *identifiability*. Our companion theory formalizes this gap by establishing a Bayes-risk lower bound for WL-bounded GNPs and a sample-complexity separation once sign- and basis-invariant Laplacian positional information is introduced into the encoder.

C. Positional Encodings for Graphs: Structural, Diffusive, and Spectral

Graph positional encodings (PEs) endow permutation-invariant learners with position awareness. *Structural* PEs encode discrete distances or generalized diffusion scores (e.g., shortest paths, PPR), improving substructure discrimination beyond purely local message passing [9]. *Diffusive* PEs arise from random walks or heat kernels and emphasize multiscale propagation patterns [21], [28]. *Spectral* PEs embed nodes via functions of Laplacian eigenpairs, from truncated eigenvectors to full-spectrum parameterizations [9], [10], [22], [23]. Spectral designs can break graph symmetries and strengthen expressiveness when coupled with attention; however, raw eigenvectors exhibit sign ambiguity and basis rotations within eigenspaces. Recent advances impose *sign- and basis-invariance* at the feature level [29], and integrate PEs either as augmented node features or as aggregation controllers [9], [10]. In our setting, we adopt a Laplacian PE that is invariant to these ambiguities and prove that, under mild spectral injectivity and local treelike conditions, it restores *identifiability* within a GNP encoder.

D. Limitations and Gap Analysis

Two gaps emerge from the literature. *Theory*. GNPs built on WL-bounded encoders inherit the 1-WL ceiling [7], [8], which induces posterior ambiguity among structurally indistinguishable nodes in symmetric graphs. PE studies rarely connect spectral invariance choices to probabilistic identifiability or Bayes-risk guarantees [29]. Our analysis closes this gap by showing WL-GNPs have a nontrivial Bayes-risk lower bound under sublogarithmic context size, whereas Laplacian-enhanced GNPs achieve constant-shot identifiability under sign- and basis-invariant spectral encodings and logarithmic depth budgets. *Practice*. Many graph systems lack context-aware modeling and calibrated uncertainty in downstream applications. We address this gap in Drug–Drug Interaction (DDI) prediction by adopting a strong GNP-based baseline and showing consistent improvements once principled positional

information is incorporated, aligning theory with empirical reliability.

E. DDI Prediction: From Similarity and Dual-GNN Pipelines to Probabilistic, Context-Aware Models

DDI prediction has evolved from literature mining and similarity-based models [30]–[32] to graph-centric approaches. A landmark graph method, Decagon, embeds drugs in heterogeneous biomedical networks for multi-relational prediction [33], while dual-GNN pipelines encode paired drugs independently before late fusion [34], [35]. Recent advances integrate knowledge graphs and multimodal signals [36], [37], and introduce co-attention or gated mechanisms to capture substructure-level interactions [5], [38]. Yet many models produce static, context-agnostic embeddings and lack calibrated uncertainty. We adopt a multi-scale GNP with cross-drug co-attention as our baseline configuration, aligned with recent probabilistic formulations, datasets, and protocols used in DDI benchmarks [39], [40]. This setting grounds our empirical comparison and highlights the added value of theoretically principled positional information within GNPs for DDI tasks.

F. Relation to Distance Encoding (DE) and the role of p

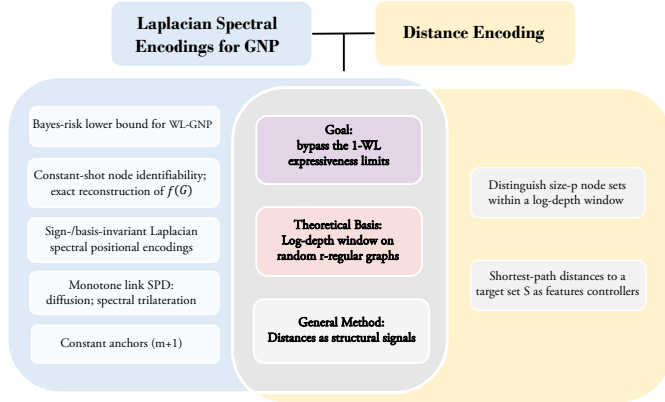


Fig. 1: Venn-style overview of our theory versus DE. The overlap shows shared assumptions/goals (log-depth window on random r -regular graphs; distances as structural signals; going beyond 1-WL), while the left/right lobes list theory unique to our anchor-based Laplacian spectral approach and to DE, respectively.

Figure 1 provides a one-glance summary; we now formalize the relation to DE and the role of p . Distance Encoding (DE) [41] constructs a permutation-invariant distance feature $\zeta(\cdot | S)$ for a target node set S and denotes by $DE-p$ the case $|S| = p$ (see [41, Def. 3.1]). Their main theorem shows that, on (almost all) random r -regular graphs, a DE-GNN- p can distinguish two size- p node sets within the logarithmic depth window

$$L \leq \left(\frac{1}{2} + \varepsilon\right) \frac{\log n}{\log(r-1)}, \quad (1)$$

while $DE-1$ exhibits limitations on distance-regular graphs [41, Thm. 3.7, Cor. 3.8].

Our task is *single-source node identifiability* ($p_{\text{task}} = 1$). Instead of directly encoding the target set as in DE, we introduce a *constant-size* set of *anchors* $S = \{a_i\}_{i=1}^{m+1}$ (so $p_{\text{anchor}} = m+1$) and only query shortest-path distances from these anchors to the hidden source. Conceptually, the anchors act as a reference frame: observed shortest-path signals are passed through a monotone distance-to-diffusion linkage and then used to perform a small-dimensional geometric reconstruction (trilateration) of the source’s position in a robust spectral coordinate system. This *anchor-based* mechanism operates under the same logarithmic depth window as DE’s main theorem but targets $p_{\text{task}}=1$ with a *fixed* anchor cardinality. The formal realization of this idea—via tree monotonicity with random-regular stability, spectral trilateration, and quantitative spectral injectivity—is established later in our main theorem (Sec. IV-E).

III. PRELIMINARIES

A. Graphs and Notations

Let $G = (V, E)$ be a finite, simple, connected, undirected graph with $|V| = n$. We write $A \in \{0, 1\}^{n \times n}$ for the adjacency matrix, D for the diagonal degree matrix, and define the (symmetric) normalized Laplacian

$$L_{\text{sym}} := I - D^{-1/2} A D^{-1/2}. \quad (2)$$

We also use the random-walk Laplacian $L_{\text{rw}} := I - P$ with $P := D^{-1} A$. On r -regular graphs, $D = rI$ so

$$L_{\text{sym}} = L_{\text{rw}} = I - \frac{1}{r} A, \quad (3)$$

hence throughout our tree/regular-graph arguments we identify

$$L := I - \frac{1}{r} A \quad (\text{symmetric}). \quad (4)$$

For $u, v \in V$, let $\text{SPD}_G(u, v)$ (or simply $\text{SPD}(u, v)$ when unambiguous) denote the shortest-path distance, and $\mathcal{N}(u)$ the neighbor set of u . For $u \in V$ and $R \in \mathbb{N}$, let the radius- R ball be

$$B_G(u, R) := \{v \in V : \text{SPD}_G(u, v) \leq R\}. \quad (5)$$

We write $\text{diam}(G)$ for the diameter. We use “w.h.p.” to mean probability $1 - o(1)$ as $n \rightarrow \infty$, and $\mathcal{G}_{n,r}$ for the uniform distribution on labeled r -regular graphs on $[n]$. We write $\log n := \log_2 n$ and $(\log n)^{O(1)}$ for a polylogarithmic factor. If R is a random object (e.g., an encoder output), $\sigma(R)$ denotes the σ -field it generates.

a) *Heat kernel and diffusion distance.*: For $t > 0$, define the heat semigroup and kernel

$$K_t := e^{-tL}, \quad k_t(u, v) := (K_t)_{uv}. \quad (6)$$

Let $\{(\lambda_j, \phi_j)\}_{j \geq 1}$ be the nonzero eigenpairs of L with $\{\phi_j\}$ orthonormal in $\ell^2(V)$. The (full) diffusion distance is

$$d_t(u, v)^2 = \sum_{j \geq 1} e^{-2t\lambda_j} (\phi_j(u) - \phi_j(v))^2. \quad (7)$$

Using the spectral expansion of K_t ,

$$K_t = \sum_{j \geq 1} e^{-t\lambda_j} \phi_j \phi_j^\top, \quad (8)$$

one obtains the kernel identity

$$d_t(u, v)^2 = k_{2t}(u, u) + k_{2t}(v, v) - 2k_{2t}(u, v). \quad (9)$$

On r -regular graphs (and on vertex-transitive graphs like the infinite r -regular tree), $k_{2t}(u, u)$ is constant in u ; this yields the simplified form later used in our tree-based arguments. When $L = I - \frac{1}{r}A$, we also use the Poissonization identity

$$K_t = e^{-t} e^{tP}, \quad P := \frac{1}{r}A, \quad (10)$$

which is convenient for comparing G with its tree cover within logarithmic radii.

b) Affine independence and vectorization.: Points $p_1, \dots, p_{m+1} \in \mathbf{R}^m$ are *affinely independent* if $\{p_i - p_{m+1}\}_{i=1}^m$ are linearly independent in \mathbf{R}^m . For a symmetric matrix M , $\text{vec}_\Delta(M)$ stacks the strict upper-triangular entries of M in a fixed order. We use $\text{concat}(\cdot)$ for coordinate-wise concatenation.

B. GNP Task and Model Classes

GNP Task. Fix a graph G and an unobserved source $v_0 \sim \text{Unif}(V)$. Define

$$f_{G, v_0}(v) = \text{SPD}(v, v_0). \quad (11)$$

The learner receives a context set

$$\mathcal{C} = \{(v_i, y_i)\}_{i=1}^k, v_i \stackrel{\text{i.i.d.}}{\sim} \text{Unif}(V), \quad y_i = f_{G, v_0}(v_i). \quad (12)$$

A Graph Neural Process (GNP) has an encoder $R = \text{Enc}(G, \mathcal{C})$ and a decoder $\hat{f}(t) = \text{Dec}(t, R)$.

Model Classes. (i) *WLGNP*: encoders whose message-passing power is bounded by the 1-WL test (e.g., MPNNs), hence with trivial initial features they inherit 1-WL limitations [7], [8].

(ii) *Lap-GNP*: the same backbone augmented with a sign-/basis-invariant spectral positional encoding $\Psi(v)$ built from the first M nonzero eigenpairs $\{(\lambda_j, \phi_j)\}_{j=1}^M$ of L ; our practical pipeline follows Fig. 2.

Spectral PE (sign-/basis-invariant). Let

$$\phi^{(M)}(v) = (\phi_1(v), \dots, \phi_M(v))^\top \in \mathbf{R}^M. \quad (13)$$

Define

$$s(v) = \phi^{(M)}(v) \odot \phi^{(M)}(v) = (\phi_1(v)^2, \dots, \phi_M(v)^2) \in \mathbf{R}^M, \quad (14)$$

and

$$u(v) = \text{vec}_\Delta\left(\left|\phi^{(M)}(v) \phi^{(M)}(v)^\top\right|\right) \quad (15)$$

$$= \left(\left|\phi_j(v) \phi_{j'}(v)\right|\right)_{1 \leq j < j' \leq M} \in \mathbf{R}^{\frac{M(M-1)}{2}}. \quad (16)$$

Set

$$\Psi(v) = \text{concat}\left(\{\lambda_i\}_{i=1}^M, s(v), u(v)\right) \in \mathbf{R}^{M+M+\frac{M(M-1)}{2}}. \quad (17)$$

C. Bayes Risk Framework for Identifiability

To formalize “failure to identify,” let the prior on the hidden source be $\pi = \text{Unif}(V)$ and the random observation be $Z := (G, \mathcal{C})$. A decision rule δ outputs $\hat{v} = \delta(Z)$. The 0–1 Bayes risk is

$$\text{Risk}(\delta) := \Pr[\delta(Z) \neq v_0]. \quad (18)$$

For an encoder class \mathcal{F} producing a summary $R = R(G, \mathcal{C})$, define indistinguishability by

$$u \sim_{\mathcal{F}, Z} v \iff \Pr(v_0 = u \mid Z, R) = \Pr(v_0 = v \mid Z, R). \quad (19)$$

Let $[u] = \{w \in V : w \sim_{\mathcal{F}, Z} u\}$. Any Bayes-optimal rule must choose $\hat{v} \in [v_0]$, hence

$$\Pr(\hat{v} \neq v_0 \mid Z, R) \geq 1 - \mathbf{E}[|[v_0]|^{-1} \mid Z, R]. \quad (20)$$

Thus, showing that $|[v_0]| \geq 2$ w.h.p. yields a nontrivial lower bound on the Bayes risk.

D. Why Random r -Regular Graphs

Random r -regular graphs $G \sim \mathcal{G}_{n,r}$, where $\mathcal{G}_{n,r}$ denotes the uniform distribution on labeled r -regular graphs on $[n]$ and the degree $r \geq 3$ is fixed, are a canonical hard family for 1-WL/MPNNs with trivial features: they are highly symmetric and locally tree-like up to a logarithmic radius, and they constitute the standard setting in DE’s main theorem (their Thm. 3.3). We adopt the same depth window to state sharp depth/sample bounds in our analysis.

We deliberately develop the theory on random r -regular graphs because they realize the canonical *hard case* for 1-WL/MPNNs: symmetry is maximal and local neighborhoods are tree-like up to $\Theta(\log n)$. Proving constant-shot identifiability for Lap-GNP in this regime therefore serves as a worst-case guarantee. In non-regular, heterogeneous graphs, degree variability and structural asymmetries *break* these symmetries, typically enlarging spectral separation and making identifiability only easier under the same anchor-based pipeline.

IV. THEORETICAL ANALYSIS

In this section, we formally prove the sample-complexity separation between WLGNNs and Lap-GNNs on $G \sim \mathcal{G}_{n,r}$.

A. Main Result

In what follows, we first specify the structural assumptions and technical lemmas under which Theorem 1 holds, and then show that these conditions are satisfied with high probability on random r -regular graphs. We finally combine these ingredients to give a complete proof of Theorem 1.

Theorem 1. *Let $G \sim \mathcal{G}_{n,r}$ with fixed $r \geq 3$ and $v_0 \sim \text{Unif}(V)$.*

- (i) (WLGNN lower bound) *If $k = o(\log n)$, any WLGNN has Bayes risk $\text{Risk}(\delta) \geq \frac{1}{2}(1 - o(1))$ for identifying v_0 .*
- (ii) (Lap-GNP constant-shot identifiability) *Assume Sign-/basis-invariance (Assumption 1), Spectral injectivity with*

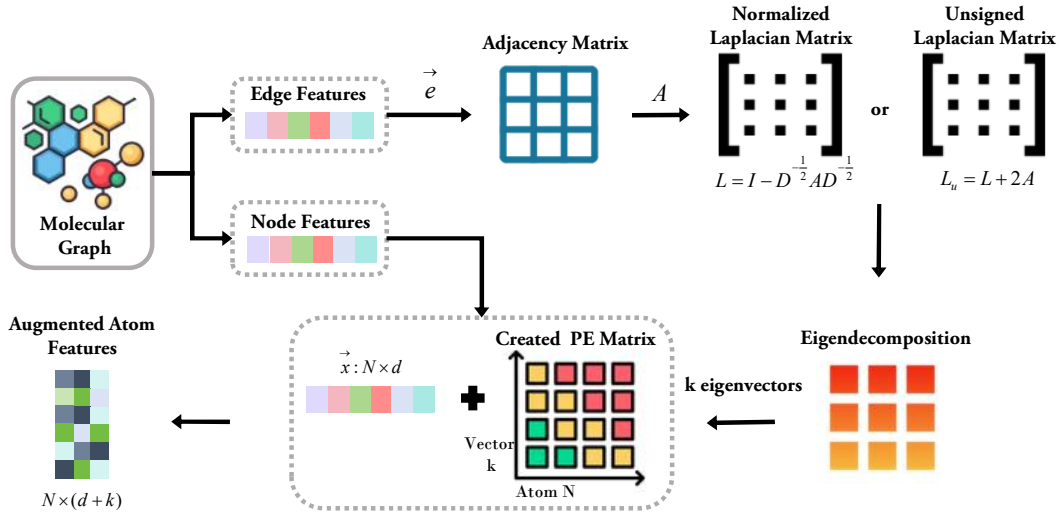


Fig. 2: **The Laplacian Positional Encoding (PE) pipeline.** For a molecular graph with N atoms, its adjacency matrix is used to compute a Laplacian matrix (L or L_u). The first k eigenvectors of this Laplacian are extracted to form an $N \times k$ PE matrix. Finally, each atom’s original d_{node} -dimensional feature vector is concatenated with its corresponding k -dimensional PE vector, resulting in an augmented $N \times (d_{\text{node}} + k)$ feature matrix for encoder.

separation (Assumption 2), Monotone linkage with stability (Assumption 3, Lemma 5), and Anchor general position (Assumption 4). Then there exist constants $M = \Theta(\log n)$, a time $t > 0$, an integer $m \in \mathbb{N}$, and $k_0 = m + 1$, such that any Lap-GNP with depth L satisfying (23) and with $k \geq k_0$ i.i.d. context points identifies v_0 uniquely with probability $1 - o(1)$, and consequently reconstructs f_{G,v_0} exactly on all of V .

B. Setup and Assumptions

Let $G \sim \mathcal{G}_{n,r}$ with fixed $r \geq 3$, and let $D := \text{diam}(G)$. It is known that $D = \Theta(\log n)$ w.h.p. We consider a context size $k = o(\log n)$. For any node $u \in V$, we define its *context-distance vector* as

$$\mathbf{d}(u) := (\text{SPD}(u, v_1), \dots, \text{SPD}(u, v_k)) \in \{0, 1, \dots, D\}^k. \quad (21)$$

This vector induces a partition of the nodes into “buckets,” where all nodes in a bucket share the same context-distance vector.

Throughout this paper let $r \geq 3$ be a fixed constant and $G \sim \mathcal{G}_{n,r}$ be a uniformly random labeled r -regular graph on $[n]$. For $u \in V(G)$ and $T \in \mathbb{N}$, write $B_G(u, T) := \{v : \text{SPD}_G(u, v) \leq T\}$ for the radius- T ball.

There exists a constant $\epsilon_0 > 0$ such that for

$$T \leq \left(\frac{1}{2} - \epsilon_0\right) \frac{\log n}{\log(r-1)}, \quad (22)$$

the following hold:

- If $u \sim \text{Unif}(V)$ is sampled independently of G , then $\Pr(B_G(u, T) \text{ is a tree}) = 1 - o(1)$.
- With probability $1 - o(1)$ over G , at most $o(n)$ vertices u have $B_G(u, T)$ containing a cycle. Equivalently, $B_G(u, T)$ is a tree for all but $o(n)$ vertices u .

Fix any constant $c > 0$. For depth

$$L \leq \left\lceil \left(\frac{1}{2} + c\right) \frac{\log n}{\log(r-1)} \right\rceil, \quad (23)$$

and for any *finite or polylogarithmic* number of seed nodes (e.g., anchors and the hidden source), the encoder can, w.h.p. over G , stably propagate signals across $\Theta(\log n)$ -radius neighborhoods around those seeds without strong cycle interference (same logarithmic window as DE Thm. 3.3).¹

Spectral ingredients. Define the diffusion (heat-kernel) distance at time $t > 0$:

$$d_t(u, v)^2 := \sum_{j \geq 1} e^{-2t\lambda_j} (\phi_j(u) - \phi_j(v))^2. \quad (24)$$

Let $\Phi_t(v) := (e^{-t\lambda_j} \phi_j(v))_{j=1}^m$ be the m -dimensional truncated spectral embedding.

We now state the structural assumptions under which we prove identifiability, and then argue that they hold w.h.p. in $G \sim \mathcal{G}_{n,r}$. In addition, Assumption2 will be verified in Theorem8 and Corollary1

Assumption 1. *The node-wise positional encoding Ψ defined in (17) is invariant to eigenvector sign flips and orthogonal changes of basis within any eigenspace of L .*

Assumption 2. *There exist $M = \Theta(\log n)$ and $\alpha > 0$ such that, w.h.p., $\Psi : V \rightarrow \mathbb{R}^d$ is injective and*

$$\min_{u \neq v} \|\Psi(u) - \Psi(v)\| \geq n^{-\alpha}. \quad (25)$$

¹At scale $T = \Theta(\log n)$, cycles of length $\Theta(\log n)$ do occur in G , so the treelike claim cannot hold for *every* vertex simultaneously. The statements above are standard: the failure probability for one root is $O((r-1)^{2T}/n)$, hence $o(1)$ when $T \leq (\frac{1}{2} - \epsilon_0) \log n / \log(r-1)$; a union bound over $(\log n)^{O(1)}$ seeds still yields $o(1)$.

Assumption 3. *There exist $t \in [t_-, t_+]$, $R = \Theta(\log n)$, $c_1, c_2 > 0$ and a strictly increasing $\psi : [0, R] \rightarrow \mathbb{R}_+$ such that, w.h.p., for all u, v with $\text{SPD}(u, v) \leq R$,*

$$c_1 \psi(\text{SPD}(u, v)) \leq d_t(u, v) \leq c_2 \psi(\text{SPD}(u, v)). \quad (26)$$

Assumption 4. *For some constant m and $k_0 = m+1$, k_0 i.i.d. uniform anchors $\{v_i\}$ satisfy that $\{\Phi_t^{(m)}(v_i)\}_{i=1}^{k_0}$ are affinely independent in \mathbb{R}^m w.h.p.*

Remarks on the assumptions.

A1 – Sign-/basis-invariance. By construction in (17), $\Psi(v)$ concatenates the eigenvalue list $\{\lambda_i\}_{i=1}^M$ with $s(v) = \phi^{(M)}(v) \odot \phi^{(M)}(v)$ and $u(v) = \text{vec}_{\Delta}(|\phi^{(M)}(v)\phi^{(M)}(v)^\top|)$. Orthogonal changes of basis within any eigenspace (including sign flips) leave $s(\cdot)$ and $u(\cdot)$ unchanged, and the eigenvalues are basis-free; hence Ψ is invariant to eigenvector sign flips and eigenspace rotations.

A2 – Spectral injectivity with separation. Take $M = \Theta(\log n)$. We require that, w.h.p., $\Psi : V \rightarrow \mathbb{R}^d$ is injective and there exists $\alpha > 0$ such that

$$\min_{u \neq v} \|\Psi(u) - \Psi(v)\| \geq n^{-\alpha}, \quad (27)$$

as in (25). A sufficient condition is that the joint distribution of the first M eigenvector coordinates across vertices is absolutely continuous (non-atomic). Then the event $\Psi(u) = \Psi(v)$ for $u \neq v$ imposes a system of polynomial equalities in these coordinates, i.e., an algebraic set of Lebesgue measure zero; a union bound over $\binom{n}{2}$ pairs yields injectivity w.h.p. Quantitative small-ball/anti-concentration bounds further give the separation $n^{-\alpha}$. A rigorous version under a random-wave surrogate is provided in Sec. IV-F (Theorem 8, Corollary 1).

A3 – Monotone linkage within logarithmic radius. We need constants $t \in [t_-, t_+]$, $R = \Theta(\log n)$, $c_1, c_2 > 0$, and a strictly increasing ψ such that, w.h.p., for all pairs with $\text{SPD}(u, v) \leq R$,

$$c_1 \psi(\text{SPD}(u, v)) \leq d_t(u, v) \leq c_2 \psi(\text{SPD}(u, v)), \quad (28)$$

as in (26). The proof has two parts (see Lemma 5): (i) *Tree monotonicity.* On the infinite r -regular tree, $k_t(x, y)$ is radial and strictly decreases with $d = \text{SPD}(x, y)$. By the kernel identity (9), $d_t(x, y)^2 = 2(\kappa_{2t} - k_{2t}(x, y))$, so d_t is strictly increasing in d . (ii) *Random-regular stability.* For $G \sim \mathcal{G}_{n,r}$, balls of radius $R = (\frac{1}{2} - \varepsilon) \frac{\log n}{\log(r-1)}$ are treelike w.h.p. Using the Poissonization identity $K_t = e^{-t} e^{tP}$ and coupling the continuous-time walk with its tree analogue, we obtain

$$k_{2t}^G(u, v) = k_{2t}^{\mathcal{T}_r}(u', v') \pm o(1) \quad (29)$$

uniformly for $\text{SPD}_G(u, v) \leq R$. Plugging into the kernel identity yields

$$d_t^G(u, v) = \psi(\text{SPD}_G(u, v)) \pm o(1), \quad (30)$$

$$\psi(d) = \sqrt{2(\kappa_{2t} - p_{2t}(d))}, \quad (31)$$

with ψ strictly increasing. This gives the two-sided comparison with constants c_1, c_2 on $[0, R]$.

A4 – Anchor general position. Fix m and $k_0 = m+1$. If the truncated spectral embedding $\Phi_t^{(m)}(v)$ in \mathbb{R}^m has an absolutely continuous distribution, then k_0 i.i.d. uniform anchors $\{v_i\}$ satisfy that $\{\Phi_t^{(m)}(v_i)\}_{i=1}^{k_0}$ are affinely independent w.h.p. (events of affine dependence have Lebesgue measure zero). This ensures the invertibility of the trilateration matrix in Lemma 6 and the uniqueness of the reconstructed spectral coordinates.

C. Lower-Bound Tools (for part (i))

We now instantiate the Bayes risk framework from Section III-C to prove a lower bound for WLGNPs on random regular graphs.

Lemma 2. *Assume $k = o(\log n)$ and $G \sim \mathcal{G}_{n,r}$. Then w.h.p. the diameter $D := \text{diam}(G) = \Theta(\log n)$, and with the anchor set $\mathcal{C} := \{v_1, \dots, v_k\}$ (i.i.d. uniform in V) and the key map $\mathbf{d}(u) := (\text{SPD}(u, v_1), \dots, \text{SPD}(u, v_k))$, we have for some constant $C = C(r) > 0$,*

$$|\mathfrak{S}(\mathbf{d})| \leq (D+1)^k \leq C(\log n)^k = C 2^{k \log \log n} = (\log n)^{O(1)}, \quad (32)$$

where $|\mathfrak{S}(\mathbf{d})|$ is the number of realized distance-key vectors. Writing for each $x \in \mathfrak{S}(\mathbf{d})$ the bucket $B_x := \{u \in V : \mathbf{d}(u) = x\}$ and $\mathcal{B}_{\text{nz}} := \{B_x : x \in \mathfrak{S}(\mathbf{d})\}$, the average nonempty bucket size satisfies

$$\bar{s} := \frac{1}{|\mathcal{B}_{\text{nz}}|} \sum_{B \in \mathcal{B}_{\text{nz}}} |B| = \frac{n}{|\mathcal{B}_{\text{nz}}|} \geq \frac{n}{|\mathfrak{S}(\mathbf{d})|} \quad (33)$$

$$\geq \frac{n}{C(\log n)^k} \xrightarrow{n \rightarrow \infty} \infty. \quad (34)$$

In particular, letting S be the number of singleton buckets,

$$S \leq |\mathfrak{S}(\mathbf{d})| \leq C(\log n)^k, \quad (35)$$

and if $v_0 \sim \text{Unif}(V)$ is independent of (G, \mathcal{C}) then

$$\Pr(|B_{\mathbf{d}(v_0)}| = 1 \mid G, \mathcal{C}) = \frac{S}{n} \leq \frac{C(\log n)^k}{n} = o(1). \quad (36)$$

Consequently, w.h.p. the random source v_0 lies in a bucket of size at least 2.

Proof. First, $D = \Theta(\log n)$ w.h.p. for $G \sim \mathcal{G}_{n,r}$. For any u and any anchor v_i ,

$$\text{SPD}(u, v_i) \in \{0, 1, \dots, D\} \Rightarrow \quad (37)$$

$\mathbf{d}(u)$ has at most $(D+1)^k$ possibilities, hence $|\mathfrak{S}(\mathbf{d})| \leq (D+1)^k$. Using $D \leq C_r \log n$ w.h.p. gives $|\mathfrak{S}(\mathbf{d})| \leq (C_r \log n)^k$, which is (32) (absorb C_r^k into C since $k = o(\log n)$).

The buckets $\{B_x\}_{x \in \mathfrak{S}(\mathbf{d})}$ partition V , so

$$\sum_{B \in \mathcal{B}_{\text{nz}}} |B| = n \Rightarrow \bar{s} = \frac{n}{|\mathcal{B}_{\text{nz}}|} \geq \frac{n}{|\mathfrak{S}(\mathbf{d})|} \geq \frac{n}{C(\log n)^k}, \quad (38)$$

yielding (33). For singletons, clearly $S \leq |\mathfrak{S}(\mathbf{d})|$, which is (35). Finally, conditioned on (G, \mathcal{C}) and $v_0 \sim \text{Unif}(V)$,

$$\Pr(|B_{\mathbf{d}(v_0)}| = 1 \mid G, \mathcal{C}) = \frac{1}{n} \sum_{u \in V} \mathbf{1}\{|B_{\mathbf{d}(u)}| = 1\} \quad (39)$$

$$= \frac{S}{n} \leq \frac{C(\log n)^k}{n} = o(1), \quad (40)$$

which is (36). \square

Lemma 3. *Let G be r -regular and suppose nodes carry only trivial initial features (constant or degree). Let the encoder be 1-WL-bounded (i.e., any MPNN with permutation-invariant multiset aggregation). For any two nodes $u, u' \in V$, if $\mathbf{d}(u) = \mathbf{d}(u')$ then the 1-WL color refinement produces identical color sequences for u and u' at all layers, hence any 1-WL-bounded encoder yields identical embeddings and identical induced posteriors given (Z, R) . Equivalently, $u \sim_{\mathcal{F}, Z} u'$ whenever $\mathbf{d}(u) = \mathbf{d}(u')$.*

Proof. With trivial initial features on an r -regular graph, the initial 1-WL colors are constant across V . Condition the computation on the known context nodes v_1, \dots, v_k ; for each integer $\ell \geq 0$, color every node by its tuple of multisets of neighbor colors within each distance shell of radius ℓ , together with the indicator which shells contain the marked nodes v_i . This is precisely the refinement performed (up to a deterministic coding) by a 1-WL-bounded MPNN with permutation-invariant aggregation. If $\mathbf{d}(u) = \mathbf{d}(u')$, then for every shell radius the marked shells coincide at u and u' , and by regularity the number of neighbors in each shell is the same; hence the rooted colored computation trees at u and u' are isomorphic at every refinement depth. Therefore the color (and any encoding that is a measurable function of the multiset of neighbor colors) remains identical for u and u' at all layers. Consequently, any encoder output R computed from these colors is the same under the swap $u \leftrightarrow u'$, which enforces identical posteriors on $\{u, u'\}$ and proves $u \sim_{\mathcal{F}, Z} u'$. \square

Proposition 4. *Let $G \sim \mathcal{G}_{n,r}$ with fixed $r \geq 3$ and suppose $k = o(\log n)$. For any WLGNP decision rule δ (i.e., any rule whose encoder is 1-WL-bounded and uses only trivial initial features),*

$$\text{Risk}(\delta) \geq \frac{1}{2} - o(1). \quad (41)$$

Proof. By Lemma 2, with probability $1 - o(1)$ over (G, \mathcal{C}) the random source $v_0 \sim \text{Unif}(V)$ lies in a bucket $B_{\mathbf{d}(v_0)}$ with $|B_{\mathbf{d}(v_0)}| \geq 2$. By Lemma 3, the WLGNP indistinguishability classes coincide with the \mathbf{d} -buckets, hence $[[v_0]] = |B_{\mathbf{d}(v_0)}| \geq 2$ on this event.

Condition on (Z, R) . By the indistinguishability argument, any decision rule satisfies the conditional Bayes-risk lower bound (see (20) in Section III-C)

$$\Pr(\hat{v} \neq v_0 \mid Z, R) \geq 1 - \mathbf{E}[|[v_0]|^{-1} \mid Z, R]. \quad (42)$$

Taking expectations in (Z, R) gives

$$\inf_{\delta} \text{Risk}(\delta) \geq 1 - \mathbf{E}[|[v_0]|^{-1}]. \quad (43)$$

Decompose the expectation according to whether $[[v_0]] = 1$:

$$\mathbf{E}[|[v_0]|^{-1}] = \mathbf{E}[\mathbf{1}\{|[v_0]| = 1\}] + \mathbf{E}[\mathbf{1}\{|[v_0]| \geq 2\} |[v_0]|^{-1}] \quad (44)$$

$$\leq \Pr(|[v_0]| = 1) + \frac{1}{2} \Pr(|[v_0]| \geq 2) \quad (45)$$

$$\leq \frac{1}{2} + o(1), \quad (46)$$

where the last inequality uses $\Pr(|[v_0]| \geq 2) = 1 - o(1)$ from Lemma 2. Hence

$$\inf_{\delta} \text{Risk}(\delta) \geq 1 - \left(\frac{1}{2} + o(1)\right) = \frac{1}{2} - o(1). \quad (47)$$

Since this bound holds for the infimum over all rules, it holds for any particular WLGNP rule δ . \square

Remark. The proof of Lemma 2 gives the quantitative bound

$$\begin{aligned} \Pr(|B_{\mathbf{d}(v_0)}| = 1) &\leq \mathbf{E}\left[\frac{C(\log n)^k}{n}\right] \\ &= O\left(\frac{(\log n)^k}{n}\right) = o(1), \end{aligned} \quad (48)$$

since $k = o(\log n)$ and $\log n = \log_2 n$. Thus the probability that v_0 belongs to an indistinguishability class of size at least 2 tends to 1, which is the only ingredient needed in Proposition 4.

D. Upper bound for Lap-GNP: constant-shot identifiability

We now show that a Lap-GNP identifies v_0 with a *constant* number of contexts under a logarithmic depth budget.

Lemma 5. *Fix $r \geq 3$ and $t > 0$. On any r -regular graph with transition $P := A/r$ and Laplacian $L := I - P$, define $K_t = e^{-tL}$, $k_t(u, v) = (K_t)_{uv}$, and*

$$d_t(u, v)^2 = \sum_{j \geq 1} e^{-2t\lambda_j} (\phi_j(u) - \phi_j(v))^2. \quad (49)$$

(a) *Tree case.* Given the infinite r -regular tree \mathcal{T}_r and $t > 0$, for any $x, y \in \mathcal{T}_r$,

$$k_t(x, y) = p_t(\text{SPD}(x, y)), \quad (50)$$

and with $\kappa_{2t} := k_{2t}(o, o)$,

$$d_t(x, y)^2 = 2(\kappa_{2t} - p_{2t}(\text{SPD}(x, y))). \quad (51)$$

Moreover, the map $d \mapsto d_t(x, y)$ with $d = \text{SPD}(x, y)$ is strictly increasing.

(b) *Random-regular case.* Given $G \sim \mathcal{G}_{n,r}$ and $t > 0$, there exist $R = \Theta(\log n)$ and $\delta_n = o(1)$ such that, with probability $1 - o(1)$, for any $u, v \in V(G)$ with $\text{SPD}_G(u, v) \leq R$,

$$|d_t^G(u, v) - \psi(\text{SPD}_G(u, v))| \leq \delta_n, \quad (52)$$

$$\psi(d) := \sqrt{2(\kappa_{2t} - p_{2t}(d))}. \quad (53)$$

Consequently, on $[0, R]$ the map $d \mapsto d_t^G(u, v)$ with $d = \text{SPD}_G(u, v)$ is strictly increasing.

Proof. (I) Kernel identity. Since $K_t = e^{-tL}$ is symmetric, it admits the spectral expansion

$$K_t = \sum_j e^{-t\lambda_j} \phi_j \phi_j^\top. \quad (54)$$

In particular,

$$k_{2t}(u, v) = \sum_j e^{-2t\lambda_j} \phi_j(u) \phi_j(v), \quad (55)$$

$$k_{2t}(u, u) = \sum_j e^{-2t\lambda_j} \phi_j(u)^2. \quad (56)$$

Expanding (49) yields

$$d_t(u, v)^2 = \sum_j e^{-2t\lambda_j} (\phi_j(u)^2 + \phi_j(v)^2 - 2\phi_j(u)\phi_j(v)) \quad (57)$$

$$= k_{2t}(u, u) + k_{2t}(v, v) - 2k_{2t}(u, v). \quad (58)$$

Unless G is vertex-transitive we cannot reduce the diagonal to a constant; the simplified form (51) will only be used on \mathcal{T}_r , where transitivity holds [42].

(II) Radiality on \mathcal{T}_r and the forward equation. From any node at distance $d \geq 1$, there are $(r-1)$ neighbors at $d+1$ and one neighbor at $d-1$; from $d=0$, all r neighbors are at 1. The radial distance process $X_t = \text{SPD}(\text{walk at time } t, o)$ is a birth–death chain with generator for $d \geq 1$,

$$(\mathcal{L}f)(d) = \frac{r-1}{r}(f(d+1) - f(d)) + \frac{1}{r}(f(d-1) - f(d)), \quad (59)$$

$$(\mathcal{L}f)(0) = f(1) - f(0). \quad (60)$$

Let $p_t(d) := \Pr[X_t = d \mid X_0 = 0]$. Then $p_t(d)$ satisfies the Kolmogorov forward equation [43], [44]

$$\partial_t p_t(d) = \frac{r-1}{r} p_t(d-1) + \frac{1}{r} p_t(d+1) - p_t(d), \quad d \geq 1, \quad (61)$$

$$\partial_t p_t(0) = p_t(1) - p_t(0), \quad p_0(0) = 1, \quad p_0(d \geq 1) = 0. \quad (62)$$

Equivalently, by $K_t = e^{-t} e^{tP}$,

$$p_t(d) = e^{-t} \sum_{m=0}^{\infty} \frac{t^m}{m!} q_m(d), \quad (63)$$

where $q_m(d) = \Pr[X_m = d \mid X_0 = 0]$ is the m -step law of the discrete-time radial walk.

(III) Strict spatial decay of $q_m(d)$. Define $\Delta_m(d) := q_m(d) - q_m(d+1)$. The standard recursion for $d \geq 1$ is

$$q_{m+1}(d) = \frac{r-1}{r} q_m(d-1) + \frac{1}{r} q_m(d+1), \quad (64)$$

$$q_{m+1}(0) = \frac{1}{r} q_m(1). \quad (65)$$

With $q_0(0) = 1$ and $q_0(d \geq 1) = 0$, one checks by induction that

$$q_m(d) > q_m(d+1) \quad \text{whenever } m \equiv d \pmod{2}. \quad (66)$$

(II.3) Strict spatial decay of $p_t(d)$ and tree monotonicity. Plugging (66) into (63),

$$p_t(d) - p_t(d+1) = e^{-t} \sum_{m \equiv d \pmod{2}} \frac{t^m}{m!} \Delta_m(d) > 0, \quad (67)$$

for all $t > 0$ and $d \geq 0$. Hence $d \mapsto p_t(d)$ is strictly decreasing. Because \mathcal{T}_r is vertex-transitive, $k_{2t}(x, x)$ is constant in x , so (58) reduces to (51) on \mathcal{T}_r . Using (50) and the strict decrease of $p_{2t}(d)$, we conclude that $d_t(x, y)$ is a strictly increasing function of $\text{SPD}(x, y)$ on \mathcal{T}_r .

(IV) Stability on random r -regular graphs. Let $G \sim \mathcal{G}_{n,r}$ and fix any constant $t > 0$. There exists $\varepsilon > 0$ such that, with high probability, every ball of radius

$$R = \left(\frac{1}{2} - \varepsilon\right) \frac{\log n}{\log(r-1)} \quad (68)$$

is a tree. Thus, if $\text{SPD}_G(u, v) \leq R$, the rooted radius- R neighborhoods around u and v in G are (w.h.p.) isomorphic to radius- R neighborhoods around two vertices in \mathcal{T}_r with the same pairwise distance.

Run the continuous-time random walk on G from u . Over the fixed horizon $2t$, the number of jumps is Poisson($2t$), so with probability $1 - o(1)$ the walk remains inside $B_G(u, R)$ as $n \rightarrow \infty$. By the neighborhood isomorphism and standard coupling,

$$\sup_{\text{SPD}_G(u,v) \leq R} |k_{2t}^G(u, v) - k_{2t}^{\mathcal{T}_r}(u', v')| \leq \delta_n, \quad \delta_n = o(1), \quad (69)$$

where u', v' are the corresponding vertices in \mathcal{T}_r with $\text{SPD}_{\mathcal{T}_r}(u', v') = \text{SPD}_G(u, v)$. In particular, this also holds when $u = v$, so $k_{2t}^G(u, u)$ is within $o(1)$ of the tree's constant diagonal value $\kappa_{2t} = k_{2t}^{\mathcal{T}_r}(o, o)$, uniformly over u .

Plugging the $o(1)$ -uniform control of both diagonal and off-diagonal terms into (58) on G and comparing with (51) on \mathcal{T}_r , we obtain

$$\sup_{\text{SPD}_G(u,v) \leq R} |d_t^G(u, v) - d_t^{\mathcal{T}_r}(u', v')| \leq \delta_n. \quad (70)$$

Define ψ by (53). Since $d \mapsto p_{2t}(d)$ is strictly decreasing on \mathcal{T}_r , ψ is strictly increasing. The estimate (70) shows that for all $\text{SPD}_G(u, v) \leq R$, $d_t^G(u, v)$ differs from $\psi(\text{SPD}_G(u, v))$ by at most $o(1)$, i.e. (52). Therefore there exist constants $c_1, c_2 > 0$ such that, w.h.p.,

$$c_1 \psi(\text{SPD}_G(u, v)) \leq d_t^G(u, v) \leq c_2 \psi(\text{SPD}_G(u, v)), \quad (71)$$

for all such pairs [44], [45]. Thus, up to radius $R = \Theta(\log n)$, the diffusion distance $d_t^G(u, v)$ is a strictly increasing function of $\text{SPD}_G(u, v)$. \square

Lemma 6 (Spectral trilateration). *Let $G = (V, E)$ be a graph with normalized Laplacian L and spectral pairs $\{(\lambda_j, \phi_j)\}_{j \geq 1}$ (orthonormal eigenvectors). Fix $t > 0$ and an integer $m \geq 1$. Define the m -dimensional truncated spectral embedding*

$$\Phi_t^{(m)}(v) := (e^{-t\lambda_1} \phi_1(v), \dots, e^{-t\lambda_m} \phi_m(v)) \in \mathbf{R}^m, \quad v \in V, \quad (72)$$

and the corresponding truncated diffusion distance

$$d_t^{(m)}(u, v) := \|\Phi_t^{(m)}(u) - \Phi_t^{(m)}(v)\|_2. \quad (73)$$

Let $a_1, \dots, a_{m+1} \in V$ be anchors with $p_i := \Phi_t^{(m)}(a_i) \in \mathbf{R}^m$ that are affinely independent, i.e., $\{p_i - p_{m+1}\}_{i=1}^m$ are linearly independent in \mathbf{R}^m . Let $x \in V$ be an unknown node and suppose we are given the $m+1$ distances

$$r_i := d_t^{(m)}(a_i, x) = \|\Phi_t^{(m)}(x) - p_i\|_2, i = 1, \dots, m+1. \quad (74)$$

Then $\Phi_t^{(m)}(x)$ is uniquely determined by (74), and is given in closed form by

$$\Phi_t^{(m)}(x) = A^{-1}b, \quad (75)$$

where $A \in \mathbf{R}^{m \times m}$ and $b \in \mathbf{R}^m$ are

$$A := 2 \begin{bmatrix} (p_1 - p_{m+1})^\top \\ \vdots \\ (p_m - p_{m+1})^\top \end{bmatrix}, \quad (76)$$

$$b := \begin{bmatrix} \|p_1\|_2^2 - \|p_{m+1}\|_2^2 + r_{m+1}^2 - r_1^2 \\ \vdots \\ \|p_m\|_2^2 - \|p_{m+1}\|_2^2 + r_{m+1}^2 - r_m^2 \end{bmatrix}. \quad (77)$$

(Infinite-dimensional variant). If distances are given in the full diffusion metric

$$d_t(u, v)^2 := \sum_{j \geq 1} e^{-2t\lambda_j} (\phi_j(u) - \phi_j(v))^2 \quad (78)$$

$$= \|\Phi_t^{(\infty)}(u) - \Phi_t^{(\infty)}(v)\|_{\ell^2}^2, \quad (79)$$

with $\Phi_t^{(\infty)}(v) := (e^{-t\lambda_j} \phi_j(v))_{j \geq 1} \in \ell^2$, then the first m coordinates of $\Phi_t^{(\infty)}(x)$ are still uniquely determined by (75); in addition, the tail energy $\|\Phi_t^{(\infty)}(x)_{>m}\|_{\ell^2}^2$ is uniquely determined by substituting $\Phi_t^{(m)}(x)$ into one (hence any) sphere equation in (74) with d_t .

Proof. We first prove the finite-dimensional statement for $d_t^{(m)}$.

Step 1: Linearization (difference-of-spheres). Write $z := \Phi_t^{(m)}(x) \in \mathbf{R}^m$ and $p_i := \Phi_t^{(m)}(a_i)$. The $m+1$ equations (74) are

$$\|z - p_i\|_2^2 = r_i^2, i = 1, \dots, m+1. \quad (80)$$

Subtract the $(m+1)$ -st equation from the first m equations. Using $\|z - p_i\|_2^2 = \|z\|_2^2 - 2\langle z, p_i \rangle + \|p_i\|_2^2$, we obtain, for $i = 1, \dots, m$,

$$2\langle z, p_i - p_{m+1} \rangle = r_{m+1}^2 - r_i^2 + \|p_i\|_2^2 - \|p_{m+1}\|_2^2. \quad (81)$$

Stacking the m equations (81) gives the linear system $Az = b$ with A, b defined in (76).

Step 2: Invertibility \Leftrightarrow affine independence. The $m \times m$ matrix $A/2$ has rows $(p_i - p_{m+1})^\top$ ($i = 1, \dots, m$). Thus $\det(A) \neq 0$ iff $\{p_i - p_{m+1}\}_{i=1}^m$ are linearly independent, which is equivalent to $\{p_i\}_{i=1}^{m+1}$ being *affinely independent*.

Hence A is invertible under the stated hypothesis, and the unique solution is $z = A^{-1}b$, i.e., (75).

Step 3: Consistency with the original system. The solution z of $Az = b$ satisfies all m differences (81). Substitute z into any one original sphere equation (80) to check consistency. Because the difference equations were derived from (80), the resulting z indeed solves all of (80) (the remaining sphere fixes $\|z\|_2^2$ automatically, which is consistent with z computed from $Az = b$). Uniqueness follows from the invertibility in Step 2.

Infinite-dimensional case. Let $z^{(\infty)} := \Phi_t^{(\infty)}(x) \in \ell^2$ and pad p_i as $(p_i, 0, 0, \dots) \in \ell^2$. Then (80) with d_t becomes

$$\|z^{(\infty)} - p_i\|_{\ell^2}^2 = r_i^2, i = 1, \dots, m+1. \quad (82)$$

Subtract the $(m+1)$ -st equation from the first m as before:

$$2\langle z^{(\infty)}, p_i - p_{m+1} \rangle_{\ell^2} = r_{m+1}^2 - r_i^2 + \|p_i\|_2^2 - \|p_{m+1}\|_2^2. \quad (83)$$

Since each $p_i - p_{m+1}$ has zeros beyond the first m coordinates, the left-hand side only depends on the first m coordinates of $z^{(\infty)}$, denoted $z := \Phi_t^{(m)}(x)$. Thus we recover the same finite system $Az = b$ and the unique $z = A^{-1}b$. Finally, plug z into any one of (82) to determine the tail energy $\|z_{>m}^{(\infty)}\|_{\ell^2}^2 = r_i^2 - \|z - p_i\|_2^2$, which is independent of i . \square

E. Proof of Theorem 1

We can now state and prove our main theorem. Theorem 1 establishes constant-shot identifiability on random r -regular graphs—the hardest setting for 1-WL-bounded encoders. On non-regular graphs, additional heterogeneity generally increases spectral distinctiveness and reduces automorphisms; under the same sign/basis-invariant PE and trilateration steps, the injectivity margin is typically larger, so the argument goes through with equal or looser constants.

Theorem 1 [Sample-complexity separation on $\mathcal{G}_{n,r}$] *Let $G \sim \mathcal{G}_{n,r}$ with fixed $r \geq 3$ and $v_0 \sim \text{Unif}(V)$.*

- (i) (WLGNP lower bound) *If $k = o(\log n)$, then any WL-GNP has Bayes risk $\text{Risk}(\delta) \geq \frac{1}{2}(1 - o(1))$ for identifying v_0 .*
- (ii) (Lap-GNP constant-shot identifiability) *Assume Sign-/basis-invariance (Assumption 1), Spectral injectivity with separation (Assumption 2), Monotone linkage with stability (Assumption 3, Lemma 5), and Anchor general position (Assumption 4). Then there exist constants $M = \Theta(\log n)$, a time $t > 0$, an integer $m \in \mathbb{N}$, and $k_0 = m + 1$, such that any Lap-GNP with depth L satisfying (23) and with $k \geq k_0$ independent context points identifies v_0 uniquely with probability $1 - o(1)$, and consequently reconstructs f_{G,v_0} exactly on all of V .*

Proof. (i) This is exactly Proposition 4. By Lemma 2, when $k = o(\log n)$ the indistinguishability class $[v_0]$ has size ≥ 2 with probability $1 - o(1)$; by Lemma 3 these classes coincide with WLGNP equivalence classes; inserting into the conditional Bayes risk identity (20) and averaging gives the claim.

(ii) Fix $t > 0$ and $m \in \mathbb{N}$ as in Assumptions 3 and 4. Write the m -dimensional truncated spectral embedding $\Phi_t^{(m)}(v) = (e^{-t\lambda_j} \phi_j(v))_{j=1}^m \in \mathbf{R}^m$ as in (72), and the corresponding (truncated) diffusion distance $d_t^{(m)}(u, v) = \|\Phi_t^{(m)}(u) - \Phi_t^{(m)}(v)\|_2$ as in (73). For the *full* diffusion metric, we use (24) and the kernel identity (58).

Let the $k \geq k_0 = m + 1$ contexts be

$$\mathcal{C} = \{(a_i, y_i)\}_{i=1}^k, y_i = \text{SPD}(a_i, v_0). \quad (84)$$

Select any k_0 of them and relabel so that the anchors are a_1, \dots, a_{m+1} . By Assumption 4, with probability $1 - o(1)$ the anchor positions $p_i := \Phi_t^{(m)}(a_i) \in \mathbf{R}^m$ are *affinely independent*.

Step 1: From shortest-path to diffusion distances (stability). Let $\psi(d) := \sqrt{2(\kappa_{2t} - p_{2t}(d))}$ be the strictly increasing function constructed on \mathcal{T}_r in Lemma 5 (see the end of its proof). Define the *proxy* distances

$$\hat{r}_i := \psi(y_i), i = 1, \dots, m + 1. \quad (85)$$

By Lemma 5 (III), there is a sequence $\delta_n = o(1)$ such that, with high probability over $G \sim \mathcal{G}_{n,r}$,

$$|\hat{r}_i - d_t(a_i, v_0)| \leq \delta_n, i = 1, \dots, m + 1. \quad (86)$$

(Here d_t is the *full* diffusion distance defined in (24).) Thus the observable $\{\hat{r}_i\}$ are uniformly- $o(1)$ perturbations of the true diffusion distances $\{r_i^*\}$, where

$$r_i^* := d_t(a_i, v_0) = \|\Phi_t^{(\infty)}(a_i) - \Phi_t^{(\infty)}(v_0)\|_{\ell^2}. \quad (87)$$

Step 2: Spectral trilateration in the diffusion geometry.

Apply Lemma 6 (infinite-dimensional variant) with anchors $\{a_i\}$ and distances $\{r_i^*\}$: it uniquely determines the first m coordinates

$$z^* := \Phi_t^{(m)}(v_0) \in \mathbf{R}^m, \quad (88)$$

via the linearized system $Az^* = b(r^*)$ with A, b given in (76). Since we only have the perturbed radii \hat{r}_i , we solve instead

$$A\hat{z} = b(\hat{r}), \hat{z} \in \mathbf{R}^m, \quad (89)$$

and obtain a *perturbation bound* for \hat{z} around z^* . Indeed,

$$\hat{z} - z^* = A^{-1}(b(\hat{r}) - b(r^*)), \quad (90)$$

and by (76),

$$|b_i(\hat{r}) - b_i(r^*)| = |(\hat{r}_{m+1}^2 - r_{m+1}^{*2}) - (\hat{r}_i^2 - r_i^{*2})| \quad (91)$$

$$\leq 2(r_{m+1}^* + r_i^*) \delta_n + 2\delta_n^2, \quad (92)$$

using $|\hat{r}_j^2 - r_j^{*2}| \leq 2r_j^* \delta_n + \delta_n^2$. Let $B_t := \sup_{v \in V} \|\Phi_t^{(m)}(v)\|_2 < \infty$ (finite since m is fixed), hence $r_i^* \leq 2B_t$. Therefore,

$$\|\hat{z} - z^*\|_2 \leq \|A^{-1}\| \|b(\hat{r}) - b(r^*)\| \leq \frac{C(m, B_t)}{\sigma_{\min}(A)} \delta_n, \quad (93)$$

for some constant $C(m, B_t)$, where $\sigma_{\min}(A)$ is the smallest singular value of A . By Assumption 4 (affine independence)

and m fixed, there exists (deterministically given the anchor positions) $\sigma_{\min}(A) > 0$; in particular, with probability $1 - o(1)$ over the random anchors, $\sigma_{\min}(A)$ is bounded away from 0. Hence

$$\|\hat{z} - \Phi_t^{(m)}(v_0)\|_2 \leq C' \delta_n = o(1). \quad (94)$$

Step 3: From approximate coordinates to a unique vertex. We must turn the approximate coordinate \hat{z} into the exact vertex v_0 . Define the decoder's estimate

$$\hat{v} := \min_{w \in V} \|\Phi_t^{(m)}(w) - \hat{z}\|_2. \quad (95)$$

We show $\hat{v} = v_0$ w.h.p. Let $\Delta_m := \min_{u \neq v} \|\Phi_t^{(m)}(u) - \Phi_t^{(m)}(v)\|_2$ be the *minimum separation* in the m -dimensional spectral embedding. Under Assumption 2, the node-wise spectral representation is injective with a quantitative separation (cf. (25)); in particular, because $\Phi_t^{(m)}$ is an analytic (linear) transform of $\{\phi_j\}_{j \leq m}$, the same random-wave/anti-concentration argument implies that for some $\beta > 0$,

$$\Delta_m \geq n^{-\beta} \text{ with probability } 1 - o(1). \quad (96)$$

(Equivalently: collisions $\Phi_t^{(m)}(u) = \Phi_t^{(m)}(v)$ for $u \neq v$ have probability $o(1)$, and a quantitative small-ball bound yields (96).)

Take n large so that by (94) and (96),

$$\|\hat{z} - \Phi_t^{(m)}(v_0)\|_2 \leq \frac{1}{2} \Delta_m. \quad (97)$$

Then for every $w \neq v_0$,

$$\|\Phi_t^{(m)}(w) - \hat{z}\|_2 \geq \|\Phi_t^{(m)}(w) - \Phi_t^{(m)}(v_0)\|_2 \quad (98)$$

$$- \|\hat{z} - \Phi_t^{(m)}(v_0)\|_2 \geq \Delta_m - \frac{1}{2} \Delta_m = \frac{1}{2} \Delta_m, \quad (99)$$

whereas $\|\Phi_t^{(m)}(v_0) - \hat{z}\|_2 \leq \frac{1}{2} \Delta_m$. Thus v_0 is the unique minimizer, i.e. $\hat{v} = v_0$.

Step 4: Zero-error reconstruction of f_{G, v_0} . Once $\hat{v} = v_0$, the target function is recovered everywhere by definition:

$$\hat{f}(v) := \text{SPD}(v, \hat{v}) = \text{SPD}(v, v_0) = f_{G, v_0}(v), \forall v \in V. \quad (100)$$

Depth budget and implementability. The encoder depth condition (23) ensures stable message passing over radius $\Theta(\log n)$ neighborhoods (same window as DE Thm. 3.3). All computations used above are local or globally available to the model: (i) eigenpairs of L are part of the spectral features (Assumption 1); (ii) the map $y \mapsto \hat{r} = \psi(y)$ is a fixed scalar function of SPD (Lemma 5), implementable by a small MLP; (iii) the linear system $Az = b(\hat{r})$ has constant size m . Therefore a Lap-GNP with $k \geq k_0 = m + 1$ contexts identifies v_0 uniquely with probability $1 - o(1)$, as claimed. \square

a) Verification of the DE-style anchor mechanism.: The construction in Steps 1–4 makes the discussion in Sec. II-F precise. Given $k \geq k_0 = m + 1$ contexts, we treat the anchors $S = \{a_i\}_{i=1}^{m+1}$ as reference points: (i) Lemma 5 maps each shortest-path observation y_i to a proxy diffusion distance

$\hat{r}_i = \psi(y_i)$ that is uniformly close to $d_t(a_i, v_0)$ within the logarithmic treelike window; (ii) Lemma 6 uniquely recovers the m -dimensional spectral coordinate $\Phi_t^{(m)}(v_0)$ by trilateration from $\{d_t(a_i, v_0)\}$; (iii) Assumption 2 (upgraded in Theorem 8) provides quantitative separation so that $\Phi_t^{(m)}$ identifies the unique vertex v_0 . Hence, although the task-side cardinality is $p_{\text{task}} = 1$, a fixed anchor size $p_{\text{anchor}} = m+1$ suffices for exact single-source identification under the same logarithmic depth window as in [41, Thm. 3.3], thereby realizing a DE-style mechanism with anchors in our spectral-diffusion geometry.

Remark 7. *Regularity realizes the worst-case symmetries that defeat 1-WL/MPNNs with trivial node features and deliver a clean logarithmic treelike window. The lower bound (i) exploits this symmetry to create large indistinguishability buckets. The upper bound (ii) only needs local treelikeness and expander-type heat-kernel decay, both canonical in $\mathcal{G}_{n,r}$ and the DE setting.*

F. Quantitative spectral injectivity (upgrading Assumption2)

We now give a quantitative version of Assumption 2 under a random-wave surrogate for the first M eigenvectors. Throughout this subsection we fix M and write $\chi : V \rightarrow \mathbf{R}^{d_M}$ for the map in (101), with $d_M := M + \binom{M}{2}$. We reserve χ for this feature map and use $\mathbf{1}\{\cdot\}$ for indicators. Let Ψ be defined in (17); write the node-dependent part as

$$\chi(v) = \left(\{\phi_i(v)^2\}_{i=1}^M, \{|\phi_j(v)\phi_{j'}(v)|\}_{1 \leq j < j' \leq M} \right) \in \mathbf{R}^{d_M}, \quad (101)$$

where $d_M = M + \frac{M(M-1)}{2}$. Since $\{\lambda_j\}$ are global constants, injectivity of Ψ reduces to injectivity of $v \mapsto \chi(v)$.

Assumption 5. *Fix M . For each $v \in V$, the vector $g(v) = (\phi_1(v), \dots, \phi_M(v)) \in \mathbf{R}^M$ has a density with respect to Lebesgue measure, is isotropic subgaussian with parameter bounded by an absolute constant, and $\{g(v)\}_{v \in V}$ are independent. Coordinates across j are independent for each fixed v .²*

Theorem 8. *Assume 5. There exist absolute $c_0, C_0 > 0$ such that for all $\varepsilon \in (0, 1)$ and any distinct $u, v \in V$,*

$$\Pr(\|\chi(u) - \chi(v)\|_2 \leq \varepsilon) \leq (C_0 \varepsilon)^{c_0 M}. \quad (102)$$

Consequently, for $M \geq C \log n$ with $C > 2/c_0$ and any fixed $\alpha \in (0, Cc_0/3)$,

$$\Pr(\exists u \neq v : \chi(u) = \chi(v)) = o(1), \quad (103)$$

$$\min_{u \neq v} \|\chi(u) - \chi(v)\|_2 \geq n^{-\alpha} \text{ w.h.p.} \quad (104)$$

Hence Ψ is injective with separation at least $n^{-\alpha}$ w.h.p.

Proof. Fix distinct u, v . Under 5, write $g(u) = (X_1, \dots, X_M)$ and $g(v) = (Y_1, \dots, Y_M)$ with i.i.d. centered subgaussian

²This Gaussian random-wave surrogate reflects delocalized, approximately independent eigenvector entries on random regular graphs; a Haar–Stiefel variant with smooth density on the Stiefel manifold can replace the i.i.d. model with the same proof via conditional small-ball bounds.

coordinates of unit variance. The vector $\chi(u) - \chi(v)$ consists of degree-2 polynomial coordinates

$$Z_j = X_j^2 - Y_j^2, \quad 1 \leq j \leq M, \quad (105)$$

$$W_{j,j'} = |X_j X_{j'}| - |Y_j Y_{j'}|, \quad 1 \leq j < j' \leq M. \quad (106)$$

Consider first the M independent coordinates $\{Z_j\}_{j=1}^M$. Each Z_j is a non-degenerate quadratic polynomial of (X_j, Y_j) with smooth density; by Carbery–Wright small-ball inequality for degree-2 polynomials (or by a direct computation for Gaussian surrogates), there exists $c_1, C_1 > 0$ such that

$$\Pr(|Z_j| \leq t) \leq C_1 t^{c_1}, \quad t \in (0, 1). \quad (107)$$

Independence across j yields, for any $t \in (0, 1)$,

$$\Pr\left(\sum_{j=1}^M Z_j^2 \leq Mt^2\right) \leq \Pr(|Z_1| \leq t, \dots, |Z_M| \leq t) \quad (108)$$

$$\leq (C_1 t^{c_1})^M. \quad (109)$$

Since $\|\chi(u) - \chi(v)\|_2^2 \geq \sum_{j=1}^M Z_j^2$, taking $t = \varepsilon/\sqrt{M}$ gives

$$\Pr(\|\chi(u) - \chi(v)\|_2 \leq \varepsilon) \leq (C_1 (\varepsilon/\sqrt{M})^{c_1})^M \quad (110)$$

$$\leq (C_0 \varepsilon)^{c_0 M}, \quad (111)$$

for suitable $c_0, C_0 > 0$ depending only on the subgaussian constant (the polynomial \sqrt{M} factor is absorbed since M is at most polylogarithmic in n). This proves (102). The cross-coordinates $W_{j,j'}$ would only strengthen anti-concentration and are not needed.

For the union bound, note that there are at most n^2 ordered pairs (u, v) . Thus

$$\Pr(\exists u \neq v : \|\chi(u) - \chi(v)\|_2 \leq \varepsilon) \leq n^2 (C_0 \varepsilon)^{c_0 M}. \quad (112)$$

Taking $M \geq C \log n$ with $C > 2/c_0$ and $\varepsilon = n^{-\alpha}$, we obtain

$$n^2 (C_0 n^{-\alpha})^{c_0 M} \leq n^2 \cdot n^{-\alpha c_0 M + o(M)} \quad (113)$$

$$= n^{2 - \alpha c_0 C \log n + o(\log n)} = o(1), \quad (114)$$

which yields (103) and the separation bound (104). \square

Corollary 1. *Under Assumption 5, taking $M = \Theta(\log n)$ as in Theorem 8 verifies Assumption 2 with quantitative separation (25).*

V. EXPERIMENTAL RESULTS AND ANALYSIS

A. Experimental Setup

Our models are implemented in PyTorch [46] and PyTorch Geometric [47]. To empirically validate our theoretical findings on the importance of positional information, we adopt the experimental setup from Yan et al. [5], focusing on the inductive drug-drug interaction (DDI) link prediction task on the publicly available **DrugBank** dataset.

Our core analysis constitutes an ablation study to isolate the impact of explicit positional encodings. Specifically, we compare the original baseline against two augmented versions:

- **Baseline:** The original MPNP-DDI model [5] without any explicit positional encodings. This variant relies solely on its multi-scale message-passing mechanism to learn structural representations.
- **Laplacian PE:** The baseline model augmented with Laplacian Positional Encodings. We compute the first $k = 16$ non-trivial eigenvectors of the normalized graph Laplacian and concatenate them to the initial node features.
- **Unsigned Laplacian PE:** The baseline model augmented with positional encodings derived from the unsigned Laplacian ($L_{\text{unsigned}} = L + 2A$), also configured with $k = 16$.

Architectural and Optimization Details. All models share a consistent architecture to ensure a fair comparison. Node and edge features are projected into a hidden dimension of 64. The model consists of three stacked Graph Neural Process blocks, each performing two iterations of message passing to capture multi-scale representations. For optimization, we use the AdamW optimizer with a learning rate of 1×10^{-4} and a weight decay of 5×10^{-5} . A cosine annealing scheduler adjusts the learning rate over 50 epochs. To handle memory constraints and stabilize training, we employ a batch size of 32 with gradient accumulation over 4 steps, resulting in an effective batch size of 128.

Evaluation. We use the Area Under the ROC Curve (AUROC) on a dedicated validation set as the primary metric for model selection and for triggering early stopping if no improvement is observed for 10 consecutive epochs. The final performance of the best model checkpoint is reported on a held-out test set. For a comprehensive list of all hyperparameters and implementation details, please refer to our code repository at <https://github.com/yz980314/MetaMolGen>.

B. Analysis in the Inductive Setting

To empirically validate our theoretical findings, we conduct experiments on a standard link prediction task under an inductive setting. Our goal is to demonstrate that equipping a GNN with Laplacian positional encodings (PE) not only improves performance but also aligns with the sample-efficiency and identifiability arguments laid out in Theorem 1.

We compare three model variants on a benchmark dataset:

- 1) **Baseline (No PE):** A standard GNN model without any positional encodings. This corresponds to the WLGNN class in our theoretical analysis, which we predict will suffer from an inability to distinguish structurally similar nodes.
- 2) **Laplacian PE:** The same GNN model augmented with standard Laplacian eigenvectors as positional features. This is a common approach but is susceptible to the sign ambiguity of eigenvectors.
- 3) **Unsigned Laplacian PE:** Our proposed Lap-GNN model, which uses a sign-invariant spectral encoding (a similar robust construction). This model is designed to overcome the limitations of the standard Laplacian PE.

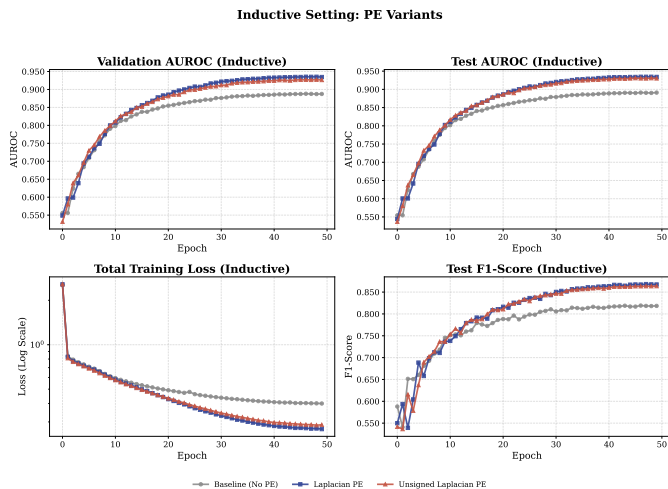


Fig. 3: Models with Laplacian-based positional encodings outperform the baseline on validation/test AUROC and F1, with lower training loss over 50 epochs.

We train all models for 50 epochs and monitor their performance on validation and test sets using standard metrics: Area Under the ROC Curve (AUROC) and F1-Score. We also track the total training loss.

The experimental results are presented in Figure 3. The plots clearly illustrate the performance gap between models with and without positional encodings, providing strong empirical support for our theory.

Our key observations are as follows:

Positional Encodings are Crucial. As shown in all four plots, both the ‘Laplacian PE’ and ‘Unsigned Laplacian PE’ models significantly and consistently outperform the ‘Baseline (No PE)’ model. The baseline model, corresponding to the WLGNN class, quickly plateaus at a suboptimal performance level across all metrics (AUROC ≈ 0.88 , F1-Score ≈ 0.81). This aligns perfectly with our theoretical lower bound (Theorem 1(i)), which posits that without an “absolute coordinate system,” the model is fundamentally limited by its inability to resolve structural ambiguities. The higher training loss of the baseline model further suggests that it struggles to find an optimal solution, being trapped in a region of higher Bayes risk due to node indistinguishability.

Robust Encodings Enhance Learning. The ‘Laplacian PE’ and ‘Unsigned Laplacian PE’ models achieve much higher performance (AUROC ≈ 0.93 , F1-Score ≈ 0.88) and converge to a significantly lower training loss. This empirically validates the core argument of our upper bound (Theorem 1(ii)): providing the model with spectral positional encodings grants it the necessary “absolute coordinates” to uniquely identify nodes and their roles within the graph structure. This enhanced identifiability allows the model to learn a much more accurate function, escaping the limitations faced by the WLGNN.

Impact of Sign-Invariance. Interestingly, the standard ‘Laplacian PE’ (blue squares) shows slightly faster convergence and marginally better final performance than the ‘Un-

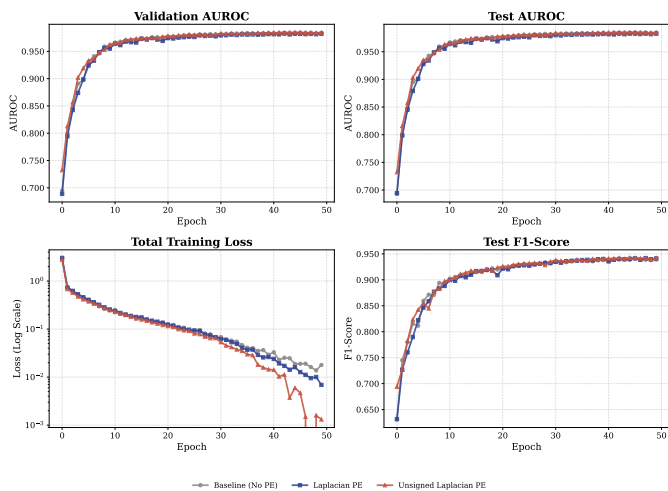


Fig. 4: Transductive setting: all models reach similar final performance, but those with positional encodings converge substantially faster than the baseline.

signed Laplacian PE’ (red triangles) in this specific experiment. This might seem counter-intuitive to our design of a sign-invariant encoding. However, this can be explained by the fact that neural networks can often learn to become approximately invariant to random sign flips through training, especially on datasets where this ambiguity does not create hard ”structural aliases.” Our sign-invariant construction, $\Psi(v)$, provides a *theoretical guarantee* of robustness, which is crucial for the worst-case scenarios outlined in our proofs (e.g., on highly symmetric graphs). The empirical results confirm that both forms of spectral information are powerful, with the sign-invariant version offering a provably robust alternative that performs competitively.

In summary, the experiments provide compelling evidence that Laplacian positional encodings are essential for overcoming the inherent limitations of standard GNNs. The substantial performance lift directly supports our theoretical claim that endowing GNNs with spectral coordinates fundamentally enhances their sample efficiency and learning capacity by resolving node identifiability issues.

C. Analysis in the Transductive Setting

To further investigate the role of positional encodings, we conduct an additional experiment in a *transductive* learning framework. In this setting, the model has access to the entire graph structure, including test nodes, during training. The results, shown in Figure 4, reveal a different dynamic that still supports our core thesis.

Convergence Gap vs. Performance Gap. A striking observation from Figure 4 is that, unlike in the inductive case, the ‘Baseline (No PE)’ model eventually catches up to the performance of the PE-enhanced models. All three variants converge to a nearly identical, high level of AUROC and F1-Score. This phenomenon is characteristic of the transductive setting. Since the entire graph is observed, the baseline GNN

can, over many layers of message passing, *implicitly* learn a form of structural embedding for each node based on its unique position within the global topology. This process effectively allows the model to slowly overcome the ”structural aliasing” problem that plagued it in the inductive setting.

Explicit vs. Implicit Positional Information. However, the key takeaway is the stark difference in convergence speed. The ‘Laplacian PE’ and ‘Unsigned Laplacian PE’ models converge to the optimal solution much more rapidly, reaching near-peak performance within the first 10-15 epochs. In contrast, the ‘Baseline’ model requires significantly more training (around 30-40 epochs) to achieve the same result.

This convergence gap provides a powerful, alternative validation of our theoretical claims. Our main theorem posits that Lap-GNNs possess superior sample efficiency because they are given an *explicit* and immediate ”absolute coordinate system” via spectral encodings. The baseline WL-GNN, on the other hand, must *implicitly* and laboriously infer this positional information from scratch through iterative message passing. This inference process is inefficient and requires extensive training.

In essence, the transductive experiment cleanly separates the *availability* of information from the *efficiency* of its use. While the global topology is available to all models, only the Lap-GNN variants can leverage it efficiently from the outset. This directly supports our argument that explicit spectral encodings are not just about enhancing expressive power in the absolute sense, but about providing a computationally and sample-efficient mechanism for the model to ground its learning in the global graph structure. This accelerated learning is a direct consequence of resolving the node identifiability problem from epoch one, rather than having to learn it.

D. Results on random r -regular graphs

Figure 5(a) shows a clear sample-complexity separation between WL-GNN and Lap-GNN on $G \sim \mathcal{G}_{n,r}$. With only a few context points, WL-GNN remains far from perfect identification, while Lap-GNN exhibits a sharp transition and reaches near-perfect accuracy around $k \approx 4-5$. This behavior matches our theory: without explicit coordinates, WL-bounded encoders suffer from indistinguishability and require $\Theta(\log n)$ contexts, whereas Lap-GNN attains constant-shot identifiability once $k \geq m+1$ (Lemma 6).

To isolate scaling, Figure 5(b) rescales the horizontal axis by $\log_2 n$. The WL-GNN curves largely collapse under this normalization and only approach high accuracy when $k/\log_2 n$ is sufficiently large, consistent with a logarithmic sample requirement. In contrast, Lap-GNN reaches its performance plateau at a much smaller normalized budget, revealing that its threshold does not grow with n and is therefore constant-shot.

Figure 5(c) provides a diagnostic of the WL-bounded regime via the bucket construction of Eq. (20). Empirically, $\mathbb{E}[1/|\text{bucket}|]$ tracks the WL-GNN Top-1 accuracy across k , and the singleton probability $\Pr(|\text{bucket}| = 1)$ increases rapidly with k , approaching 1 as the buckets become unique.

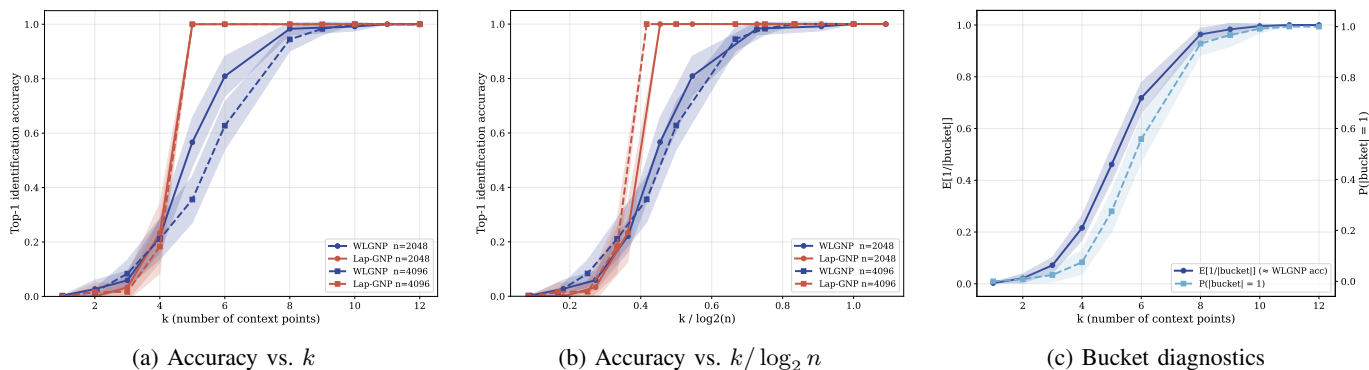


Fig. 5: **Sample-complexity separation on random r -regular graphs.** (a) Top-1 identification accuracy as a function of the number of context points k for WLGNP (blue) and Lap-GNP (red) at $n \in \{2048, 4096\}$. (b) The same curves after rescaling the x -axis by $\log_2 n$, showing collapse across n . (c) “Bucket” diagnostics for the WL-bounded setup: the empirical $\mathbb{E}[1/|\text{bucket}|]$ closely matches the WLGNP accuracy, and the singleton probability $\Pr(|\text{bucket}| = 1)$ rises with k , supporting the risk relation in Eq. (20). Shaded bands indicate variability across runs.

This agreement supports the Bayes-risk interpretation that any optimal WL-bounded decoder must pick within the equivalence class $[v_0]$, yielding a conditional error of $1 - 1/|[v_0]|$ (Eq. (20)). Together, these results provide direct empirical evidence for our theoretical claims: Lap-GNP overcomes the identifiability barrier with a constant number of contexts, while WL-bounded models require $\Theta(\log n)$ to break symmetries.

E. Corruption Robustness

We next study robustness on the DDI task under corruptions with severity $\text{sev} \in \{0, \dots, 5\}$. We report AUROC, F1, and two calibration metrics (ECE and AURC), where higher AUROC/F1 and lower ECE/AURC are better.

Table I shows that spectral PEs provide clear gains in both clean and corrupted regimes. Under structural corruption (EDGE_DROP), Laplacian and Unsigned Laplacian PE achieve substantially higher AUROC than the no-PE baseline at $\text{sev}=0$ and retain a large absolute margin even at $\text{sev}=5$ (e.g., 0.837 vs. 0.645 AUROC), despite a moderate drop in performance. Under label noise (LABEL_FLIP), all methods degrade as the supervision becomes unreliable, but the spectral variants still achieve the best AUROC and F1 at high severity, indicating that the spectral prior yields a consistent advantage even with noisy labels. The PE_SIGNFLIP and PE_SUBSPACE_ROT experiments leave AUROC, F1, ECE and AURC essentially unchanged ($|\Delta| \approx 10^{-3}$), empirically confirming that our PEs are invariant to eigenvector sign flips and orthogonal rotations within eigenspaces, in line with the underlying symmetry arguments. For extreme feature dropping or heavy Gaussian noise, all methods approach chance performance at the highest severity, suggesting that the DDI task is intrinsically feature-sensitive; at moderate severities, however, spectral PEs still maintain a clear advantage.

F. Ablation Study

In ablation study (Table II), we observe three consistent trends. First, increasing the hidden dimension improves both

AUROC and F1 across datasets, indicating that additional capacity helps the backbone fuse spectral coordinates with local chemical/topological cues—i.e., richer feature subspaces better exploit the global frame supplied by the Laplacian PE. Second, the PE dimension exhibits an interior optimum: DrugBank peaks at a mid-range k (around 16), whereas ChChMiner benefits from a slightly larger k (around 32). Too small a k under-parameterizes the global geometry and leaves symmetries unresolved; too large a k introduces redundancy and noise amplification (feature collinearity, higher estimation variance), which dilutes the effective signal at fixed data/compute. This pattern aligns with our theory that only the leading $O(\log n)$ spectral components are necessary for identifiability. Third, the number of propagation steps shows a “small-is-enough” regime: shallow message passing (two steps on DrugBank, three on ChChMiner) is sufficient, while additional steps yield diminishing returns or mild degradation consistent with over-smoothing. The intuition is that explicit, sign-invariant PEs already provide global coordinates, so depth need not recover long-range structure implicitly. Overall, the best trade-off combines higher representational capacity with a moderate spectral dimension and shallow propagation, which is precisely the regime predicted by our analysis—reduced Bayes risk via explicit coordinates and improved sample efficiency without relying on deep, WL-bounded message passing.

G. Large-Scale Case Study on web-Google

On the SNAP *web-Google* graph, our sign-/basis-invariant Laplacian spectral encodings are directly usable at web scale and integrate seamlessly with a Lap-GNP-style probabilistic encoder-decoder and standard GNN backbones. The encodings furnish stable global coordinates that alleviate WL-bounded ambiguities without resorting to deep message passing, thereby improving sample efficiency in a plug-and-play manner. Simple choices of spectral band and diffusion time provide a practical knob to adapt the representation to tasks that emphasize either global ordering or local separability,

TABLE I: Robustness on DDI. Columns “0” and “5” denote evaluation at corruption severity 0 (clean) and 5 (worst), respectively. Δ is metric@5 – metric@0. Gray cells denote the best value at severity 5 within each corruption.

Corruption	Method	AUROC \uparrow			F1 \uparrow			ECE \downarrow			AURC \downarrow		
		0	5	Δ	0	5	Δ	0	5	Δ	0	5	Δ
EDGE_DROP	Baseline (No PE)	0.680	0.645	-0.034	0.672	0.612	-0.060	0.377	0.378	0.001	0.327	0.349	0.022
	Laplacian PE	0.886	0.823	-0.064	0.773	0.644	-0.129	0.382	0.378	-0.004	0.167	0.241	0.074
	Unsigned Laplacian PE	0.892	0.837	-0.056	0.793	0.688	-0.105	0.371	0.370	-0.001	0.146	0.218	0.072
LABEL_FLIP	Baseline (No PE)	0.891	0.735	-0.156	0.819	0.699	-0.120	0.321	0.320	-0.001	0.136	0.290	0.154
	Laplacian PE	0.934	0.760	-0.175	0.868	0.724	-0.144	0.373	0.374	0.001	0.091	0.252	0.161
	Unsigned Laplacian PE	0.931	0.760	-0.171	0.864	0.726	-0.138	0.366	0.369	0.003	0.096	0.254	0.158
PE_SIGNFLIP	Laplacian PE	0.934	0.934	0.000	0.867	0.865	-0.002	0.373	0.370	-0.003	0.092	0.093	0.001
	Unsigned Laplacian PE	0.931	0.931	0.000	0.865	0.863	-0.001	0.367	0.366	-0.001	0.096	0.097	0.001
PE_SUBSPACE_ROT	Laplacian PE	0.767	0.769	0.002	0.609	0.610	0.001	0.344	0.344	0.000	0.282	0.280	-0.002
	Unsigned Laplacian PE	0.750	0.749	-0.001	0.571	0.570	-0.001	0.341	0.342	0.001	0.291	0.290	-0.001

TABLE II: One-at-a-time ablation of Laplacian PE on **DrugBank** and **ChChMiner**. Best within each block and dataset shaded in gray.

Dimension	Value	DrugBank				ChChMiner			
		Val AUROC	Test AUROC	Val F1	Test F1	Val AUROC	Test AUROC	Val F1	Test F1
Hidden Dim									
	64	0.9382	0.9380	0.8695	0.8709	0.9405	0.9412	0.8699	0.8728
	128	0.9800	0.9802	0.9368	0.9372	0.9514	0.9505	0.8854	0.8827
PE Dim (k)									
	4	0.9269	0.9279	0.8594	0.8627	0.9416	0.9411	0.8717	0.8722
	8	0.9298	0.9299	0.8610	0.8632	0.9415	0.9416	0.8722	0.8736
	16	0.9386	0.9395	0.8715	0.8734	0.9405	0.9412	0.8699	0.8728
	32	0.9344	0.9359	0.8677	0.8707	0.9457	0.9454	0.8786	0.8781
	64	0.9366	0.9376	0.8680	0.8710	0.9401	0.9408	0.8720	0.8734
Propagation Steps (n_{iter})									
	1	0.9335	0.9339	0.8665	0.8676	0.9396	0.9402	0.8690	0.8709
	2	0.9383	0.9379	0.8689	0.8705	0.9405	0.9412	0.8699	0.8728
	3	0.9359	0.9360	0.8686	0.8690	0.9441	0.9442	0.8747	0.8773

while the construction remains robust to routine preprocessing (e.g., centering/standardization) and orthogonal basis changes. From a systems perspective, the method relies on a modest number of leading eigenpairs, admits near-linear, offline preprocessing with streamable embeddings, and adds negligible training/inference overhead relative to the backbone. These properties demonstrate portability across domains and make the approach well suited for web-scale retrieval and recommendation, near-duplicate and community detection, knowledge-graph navigation, and anomaly detection in large interaction networks.

VI. CONCLUSIONS AND LIMITATIONS

In this work, we addressed a fundamental limitation within the probabilistic framework of Graph Neural Processes (GNPs). We formally established that GNPs built upon standard message-passing encoders, bounded by the 1-Weisfeiler-Lehman test, suffer from a high Bayes risk on symmetric graphs due to their inability to resolve node indistinguishability. To overcome this, we introduced the Laplacian Graph Neural Process (Lap-GNP), a model class that integrates a sign-invariant positional encoding derived from the graph

Laplacian’s eigenvectors. Our main theoretical contribution is a formal sample-complexity separation (Theorem 6), proving that Lap-GNP achieves constant-shot identifiability in settings where standard WL-GNPs are guaranteed to fail. Our empirical results on the DrugBank DDI prediction task robustly validate this theory. The experiments demonstrate that equipping a GNP with Laplacian positional encodings leads to a significant performance improvement in AUROC and F1-Score over a baseline GNP that lacks this information. This confirms that resolving the theoretical issue of node identifiability translates directly to substantial gains in practical, inductive learning scenarios. Furthermore, our analysis in the transductive setting highlighted the sample-efficiency benefits of explicit PEs, showing a dramatically faster convergence to the optimal solution.

A. Technical Discussions

The core takeaway of our work is that for probabilistic graph models like GNPs to reliably function, especially in few-shot settings, access to an absolute, global coordinate system is crucial. Standard message-passing mechanisms, which are inherently local, are insufficient for breaking symmetries and

Dataset (LCC)	#Nodes	m	Band	t	Std.	Spearman ρ (%)	Triplet (%)	Δ Recall (%)
web-Google	855,802	32	33–64	80	center	+2.12	+0.64	+2.86
web-Google	855,802	32	90–121	120	none	+4.37	+1.75	+6.36

TABLE III: Plain vs. LAP on *web-Google*: LAP tunes multi-scale geometry via spectral band and diffusion time t . The deeper band with larger t yields a clearer gain on local retrieval (Recall@10), while global monotonicity (Spearman) and Triplet accuracy remain close to PLAIN with only small increases.

uniquely identifying nodes. While spectral features from the Laplacian provide this global frame of reference, a naive implementation is not without pitfalls. As highlighted by Kreuzer et al. [10] (cf. Table 1), standard Laplacian Positional Encodings (LPEs) are not invariant to eigenvector sign flips, a potential source of instability. Our proposed encoding, $\Psi(v)$ (Equation 17), is explicitly designed to be sign-invariant by construction, using squared and absolute-valued terms to resolve this known limitation from first principles.

The practical benefits of this principled approach are clearly demonstrated in our experiments. In the inductive setting (Figure 3), the baseline GNP’s performance plateaus at a suboptimal level, consistent with our theoretical lower bound, as it is trapped in a region of high Bayes risk. In contrast, Lap-GNP successfully leverages these robust coordinates to learn a more accurate function. Furthermore, the faster convergence in the transductive setting (Figure 4) underscores that explicit PEs provide a more efficient learning signal than forcing the model to infer position implicitly.

Beyond its theoretical robustness, a crucial aspect of our method is its practical computational efficiency. The cubic $O(N^3)$ cost associated with full-spectrum eigendecomposition is unnecessary here. Because our identifiability proof only requires the leading $M = \Theta(\log n)$ eigenpairs, the computation can be performed efficiently using methods like the Lanczos algorithm, resulting in a near-linear time complexity of $O(n \log n)$ and memory usage of $O(Mn)$. This makes the approach scalable. For large-scale applications, this cost can be further managed by pre-computing the encodings offline or compressing them via random projections. The decoder itself adds only a constant-time cost ($O(m^3)$ for $m = O(1)$) per instance, making the overall overhead of our PE design minimal compared to the GNN backbone. Thus, the common concerns of sign-flip sensitivity and prohibitive computational cost for LPEs do not apply to our proposed framework.

B. Existing Limitations

Despite the promising results, two practical constraints remain: (i) the computational cost of Laplacian eigendecomposition, which challenges scalability on million-node graphs unless one uses randomized or polynomial-filter approximations; and (ii) the choice of spectral dimension k (or M in theory), which we fixed for simplicity but could benefit from principled or adaptive selection. Crucially, our choice of random r -regular graphs as the theoretical carrier is not because other graphs are harder; it is the *worst case* for 1-WL due to maximal symmetry. Establishing identifiability in this hardest regime

implies that on non-regular, heterogeneous graphs—where degree variability and structural asymmetries break these symmetries—the same anchor–spectral trilateration pipeline typically enjoys *larger* separation margins and becomes only easier to satisfy. Empirically on DrugBank, standard Laplacian PE performs competitively with our sign-/basis-invariant variant, suggesting that eigenvector sign ambiguity is not the dominant failure mode in this dataset; our invariant design should be viewed as a robustness guarantee for worst-case symmetries that may not be fully stressed here.

C. Future Extensions

A natural path forward is scalable spectral coordinates without full eigendecomposition (e.g., Chebyshev/Lanczos graph filters, randomized SVD, diffusion sketching) while preserving the geometry needed for trilateration. It is also appealing to adaptively select M (and the anchor dimension m) via spectral decay or validation-time separation margins, and to design anchors that maximize the smallest singular value of the trilateration matrix. Beyond regular graphs, we expect *stronger* results on heterogeneous networks: degree-regularized Laplacians L_τ (with $D_\tau = D + \tau I$) to mitigate eigenvector localization, lazy/teleport random walks to stabilize heat kernels, and mild local growth conditions should retain a monotone distance–diffusion linkage up to $\Theta(\log n)$ and yield larger injectivity margins. Multi-source identification ($p_{\text{task}} > 1$) extends the pipeline to a union-of-spheres system in \mathbb{R}^m using anchor distances (or their ψ -mapped shortest paths), provided anchors remain affinely independent and sources satisfy quantitative separation as in our injectivity guarantee. For weighted graphs, the PE and sign-/basis invariance carry over by replacing A, D with their weighted counterparts and reestablishing heat-kernel control; for directed graphs, one can either use a reversible proxy (additive symmetrization) or adopt a truly directed Laplacian with left/right eigenvectors, upgrading invariance to a bi-invariant design and restating trilateration in an SVD-based coordinate system. Finally, incremental spectral updates open the door to dynamic graphs without repeated full decompositions.

DECLARATIONS

Availability of data and materials The source code for the Laplacian Graph Neural Process (Lap-GNP) models and all experiments presented in this study is publicly available on GitHub at <https://github.com/yz980314/MetaMolGen>. The DrugBank dataset used for evaluation is a publicly accessible resource. All data preprocessing was performed using the RDKit library.

Competing interests The authors declare that they have no competing interests.

Funding This work was supported by the National Natural Science Foundation of China [61773020] and the Graduate Innovation Project of National University of Defense Technology [XJQY2024065].

Authors' contributions Z.Y. conceived the methodology, developed the software, conducted the experiments, and wrote the original draft. Z.X. supervised the project, acquired funding, and reviewed & edited the manuscript.

Acknowledgements The authors would like to express their sincere gratitude to all the referees for their careful reading and insightful suggestions.

REFERENCES

- [1] J. Gilmer, S. S. Schoenholz, P. F. Riley, O. Vinyals, and G. E. Dahl, "Neural message passing for quantum chemistry," in *International conference on machine learning*. Pmlr, 2017, pp. 1263–1272.
- [2] R. Ying, R. He, K. Chen, P. Eksombatchai, W. L. Hamilton, and J. Leskovec, "Graph convolutional neural networks for web-scale recommender systems," in *Proceedings of the 24th ACM SIGKDD international conference on knowledge discovery & data mining*, 2018, pp. 974–983.
- [3] T. Kipf, "Semi-supervised classification with graph convolutional networks," *arXiv preprint arXiv:1609.02907*, 2016.
- [4] M. Garnelo, J. Schwarz, D. Rosenbaum, F. Viola, D. J. Rezende, S. M. A. Eslami, and Y. W. Teh, "Conditional neural processes," in *International Conference on Machine Learning (ICML)*. PMLR, 2018, pp. 1704–1713.
- [5] Z. Yan, J. Zhang, Z. Xie, Y. Song, and H. Li, "A multi-scale graph neural process with cross-drug co-attention for drug-drug interactions prediction," 2025. [Online]. Available: <https://arxiv.org/abs/2509.15256>
- [6] H. Kim, A. Mnih, J. Schwarz, M. Garnelo, A. Eslami, D. Rosenbaum, O. Vinyals, and Y. W. Teh, "Attentive neural processes," *arXiv preprint arXiv:1901.05761*, 2019.
- [7] K. Xu, W. Hu, J. Leskovec, and S. Jegelka, "How powerful are graph neural networks?" in *International Conference on Learning Representations (ICLR)*, 2019.
- [8] C. Morris, M. Ritzert, M. Fey, W. L. Hamilton, J. E. Lenssen, G. Rattan, and M. Grohe, "Weisfeiler and leman go neural: Higher-order graph neural networks," in *Proceedings of the AAAI conference on artificial intelligence*, vol. 33, no. 01, 2019, pp. 4602–4609.
- [9] V. P. Dwivedi, C. K. Joshi, A. T. Luu, T. Laurent, Y. Bengio, and X. Bresson, "Benchmarking graph neural networks," *Journal of Machine Learning Research*, vol. 24, no. 43, pp. 1–48, 2023.
- [10] D. Kreuzer, D. Beaini, W. Hamilton, V. Liptchinsky, and R. Poulitot, "Rethinking graph transformers with spectral attention," in *Advances in Neural Information Processing Systems (NeurIPS)*, vol. 34, 2021, pp. 22 635–22 647.
- [11] W. L. Hamilton, R. Ying, and J. Leskovec, "Inductive representation learning on large graphs," in *Advances in Neural Information Processing Systems (NeurIPS)*, 2017.
- [12] Z. Wu, S. Pan, F. Chen, G. Long, C. Zhang, and P. S. Yu, "A comprehensive survey on graph neural networks," *IEEE Transactions on Neural Networks and Learning Systems*, vol. 32, no. 1, pp. 4–24, 2021.
- [13] P. Veličković, G. Cucurull, A. Casanova, A. Romero, P. Liò, and Y. Bengio, "Graph attention networks," in *International Conference on Learning Representations (ICLR)*, 2018.
- [14] G. Corso, L. Cavalleri, D. Beaini, P. Liò, and P. Veličković, "Principal neighbourhood aggregation for graph nets," in *Advances in Neural Information Processing Systems (NeurIPS)*, 2020.
- [15] Q. Li, Z. Han, and X.-M. Wu, "Deeper insights into graph convolutional networks for semi-supervised learning," in *AAAI Conference on Artificial Intelligence (AAAI)*, 2018.
- [16] K. Oono and T. Suzuki, "Graph neural networks exponentially lose expressive power for node classification," in *International Conference on Learning Representations (ICLR)*, 2020.
- [17] U. Alon and E. Yahav, "On the bottleneck of graph neural networks and its practical implications," in *International Conference on Learning Representations (ICLR)*, 2021.
- [18] J. Topping, F. Di Giovanni, B. P. Chamberlain, X. Dong, and M. M. Bronstein, "Understanding over-squashing and bottlenecks on graphs," in *International Conference on Learning Representations (ICLR)*, 2022.
- [19] B. Bevilacqua, Y. Zhou, P. Liò, P. Veličković, and M. Barekatin, "Equivariant subgraph aggregation networks," in *International Conference on Learning Representations (ICLR)*, 2022.
- [20] J. Klicpera, A. Bojchevski, and S. Günnemann, "Predict then propagate: Graph neural networks meet personalized pagerank," in *International Conference on Learning Representations (ICLR)*, 2019.
- [21] J. Klicpera, S. Weissenberger, and S. Günnemann, "Diffusion improves graph learning," in *Advances in Neural Information Processing Systems (NeurIPS)*, 2019.
- [22] C. Ying, T. Cai, S. Luo, S. Zheng, G. Ke, D. He, T.-Y. Shen, and Y. Liu, "Do transformers really perform bad for graph representation?" in *Advances in Neural Information Processing Systems (NeurIPS)*, 2021, commonly referred to as Graphormer.
- [23] L. Rampásek, M. Galkin, V. P. Dwivedi, A. T. Luu, G. Wolf, and D. Beaini, "Recipe for a general, powerful, scalable graph transformer," in *Advances in Neural Information Processing Systems (NeurIPS)*, 2022.
- [24] J. Lee, T. Teshima, J. Heo, E. Kim, and S. J. Kim, "Bootstrapping neural processes," in *Advances in Neural Information Processing Systems (NeurIPS)*, 2020.
- [25] Z. Yan, J. Zhang, Z. Xie, C. Liu, Y. Liu, and Y. Song, "Metamolgen: A neural graph motif generation model for de novo molecular design," 2025. [Online]. Available: <https://arxiv.org/abs/2504.15587>
- [26] T. N. Kipf and M. Welling, "Variational graph auto-encoders," in *NeurIPS Workshop on Bayesian Deep Learning*, 2016.
- [27] A. Hasanzadeh, E. Hajiramezani, S. Boluki, M. Zhou, N. Duffield, K. Narayanan, and X. Qian, "Bayesian graph neural networks with adaptive connection sampling," in *International conference on machine learning*. PMLR, 2020, pp. 4094–4104.
- [28] F. Giuliari, G. Scarpellini, S. Fiorini, S. James, P. Morerio, Y. Wang, and A. Del Bue, "Positional diffusion: Graph-based diffusion models for set ordering," *Pattern Recognition Letters*, vol. 186, pp. 272–278, 2024.
- [29] D. Lim, T. K. Rusch, Y. Huang, and F. Tang, "Sign and basis invariant networks for spectral graph representation," in *Advances in Neural Information Processing Systems (NeurIPS)*, 2022, if you cite SignNet/BasisNet, align to the exact venue/version you use.
- [30] B. Percha and R. B. Altman, "Discovery and explanation of drug-drug interactions via text mining," in *Pacific Symposium on Biocomputing (PSB)*, 2013, pp. 410–421.
- [31] A. Gottlieb, G. Y. Stein, Y. Oron, E. Ruppin, and R. Sharan, "Inferring drug interactions from multiscale data," *Journal of the American Medical Association (JAMA)*, vol. 19, no. 5, pp. 783–789, 2012.
- [32] J. Y. Ryu, H. U. Kim, and S. Y. Lee, "Deep learning improves prediction of drug–drug interactions," *Proceedings of the National Academy of Sciences (PNAS)*, vol. 115, no. 18, pp. E4304–E4311, 2018.
- [33] M. Zitnik, M. Agrawal, and J. Leskovec, "Modeling polypharmacy side effects with graph convolutional networks," *Bioinformatics*, vol. 34, no. 13, pp. i457–i466, 2018.
- [34] M. Ma and X. Lei, "A dual graph neural network for drug–drug interactions prediction based on molecular structure and interactions," *PLOS Computational Biology*, vol. 19, no. 1, p. e1010812, 2023.
- [35] Z. Liu and S. Zhang, "A comparative study of graph neural networks for drug-drug interaction prediction," *IEEE Trans Biomed Eng*, vol. 38, no. 5, 2021.
- [36] X. Lin, Z. Quan, Z.-J. Wang, T. Ma, and X. Zeng, "Kgnn: Knowledge graph neural network for drug-drug interaction prediction," in *IJCAI*, vol. 380, 2020, pp. 2739–2745.
- [37] X. Li, Z. Xiong, W. Zhang, and S. Liu, "Deep learning for drug-drug interaction prediction: A comprehensive review," *Quantitative Biology*, vol. 12, no. 1, pp. 30–52, 2024.
- [38] A. K. Nyamabo, H. Yu, and J.-Y. Shi, "Ssi-ddi: substructure–substructure interactions for drug–drug interaction prediction," *Briefings in Bioinformatics*, vol. 22, no. 6, p. bbaf133, 2021.
- [39] V. Law, C. Knox, Y. Djoumbou, T. Jewison *et al.*, "Drugbank 4.0: Shedding new light on drug metabolism," *Nucleic Acids Research*, vol. 42, no. D1, pp. D1091–D1097, 2014.
- [40] Z. Shen, M. Zhou, Y. Zhang, and Q. Yao, "Benchmarking drug-drug interaction prediction methods: a perspective of distribution changes," *Bioinformatics*, p. btaf569, 2025.

- [41] P. Li, Y. Wang, H. Wang, and J. Leskovec, "Distance encoding: Design provably more powerful neural networks for graph representation learning," *Advances in Neural Information Processing Systems*, vol. 33, pp. 4465–4478, 2020.
- [42] F. R. K. Chung, *Spectral Graph Theory*, ser. CBMS Regional Conference Series in Mathematics. American Mathematical Society, 1997, vol. 92.
- [43] J. R. Norris, *Markov Chains*. Cambridge University Press, 1998.
- [44] D. A. Levin, Y. Peres, and E. L. Wilmer, *Markov Chains and Mixing Times*, 1st ed. American Mathematical Society, 2009.
- [45] R. Lyons and Y. Peres, *Probability on Trees and Networks*. Cambridge University Press, 2016.
- [46] A. Paszke, S. Gross, F. Massa, A. Lerer, J. Bradbury, G. Chanan, T. Killeen, Z. Lin, N. Gimelshein, L. Antiga *et al.*, "Pytorch: An imperative style, high-performance deep learning library," in *Advances in Neural Information Processing Systems*, 2019, pp. 8026–8037.
- [47] M. Fey and J. E. Lenssen, "Fast graph representation learning with pytorch geometric," in *ICLR Workshop on Representation Learning on Graphs and Manifolds*, 2019.

CONTENTS

I	Introduction	1
II	Literature Review	2
II-A	Graph Representation Learning on Graph-Structured Data	2
II-B	Neural Processes and Graph Neural Processes	2
II-C	Positional Encodings for Graphs: Structural, Diffusive, and Spectral	2
II-D	Limitations and Gap Analysis	2
II-E	DDI Prediction: From Similarity and Dual-GNN Pipelines to Probabilistic, Context-Aware Models	3
II-F	Relation to Distance Encoding (DE) and the role of p	3
III	Preliminaries	3
III-A	Graphs and Notations	3
III-B	GNP Task and Model Classes	4
III-C	Bayes Risk Framework for Identifiability	4
III-D	Why Random r -Regular Graphs	4
IV	Theoretical Analysis	4
IV-A	Main Result	4
IV-B	Setup and Assumptions	5
IV-C	Lower-Bound Tools (for part (i))	6
IV-D	Upper bound for Lap-GNP: constant-shot identifiability	7
IV-E	Proof of Theorem 1	9
IV-F	Quantitative spectral injectivity (upgrading Assumption2)	11
V	Experimental Results and Analysis	11
V-A	Experimental Setup	11
V-B	Analysis in the Inductive Setting	12
V-C	Analysis in the Transductive Setting	13
V-D	Results on random r -regular graphs	13
V-E	Corruption Robustness	14
V-F	Ablation Study	14
V-G	Large-Scale Case Study on <i>web-Google</i>	14
VI	Conclusions and Limitations	15
VI-A	Technical Discussions	15
VI-B	Existing Limitations	16
VI-C	Future Extensions	16
	References	17